Computers and Structures 228 (2020) 106146

Contents lists available at ScienceDirect

Computers and Structures

journal homepage: www.elsevier.com/locate/compstruc

Efficient topology optimization of multicomponent structure using substructuring-based model order reduction method

Hyeong Seok Koh, Jun Hwan Kim, Gil Ho Yoon *

Mechanical Engineering, Hanyang University, Republic of Korea

ARTICLE INFO

Article history:
Received 12 July 2019
Accepted 28 October 2019
Available online 18 November 2019

Keywords:
Topology optimization
Model reduction schemes
Substructure design
Krylov subspace
Ritz vector method

ABSTRACT

This study develops a novel model reduction (MR) scheme called the multi-substructure multi-frequency quasi-static Ritz vector (MMQSRV) method to compute dynamic responses and sensitivity values with adequate efficiency and accuracy for topology optimization (TO) of dynamic systems with multiple substructures. The calculation of structural responses of dynamic excitation using the framework of the finite element (FE) procedure usually requires a significant amount of computation time. The ever-increasingly complex phenomena of FE models with many degrees of freedom make it difficult to calculate FE responses in the time or frequency domain. To overcome this difficulty, model reduction schemes can be utilized to reduce the size of the dynamic stiffness matrix. This paper presents a new model order reduction method called MMQSRV, based on the quasi-static Ritz vector method, with Krylov subspaces spanned at multiple angular velocities for efficient TO. Through several analysis and design examples, we validate the efficiency and reliability of the model reduction schemes for TO.

1. Introduction

This study developed a novel model reduction (MR) scheme and investigated how the dynamic characteristics of multicomponent structures could be efficiently improved through the density-based topology optimization. For a long time improving the vibration or noise characteristics of structure by changing its geometry has been a subject of research and discussion for engineers and scientists [1,2]. To improve these characteristics systematically via finite element (FE) method, topology optimizations have been developed and applied to various engineering problems [2,5,6,10,11,14,17–20,22–26,28–33]. However, despite the interest in topology optimization for dynamic structures, the very high computation time required for the optimization process often becomes a huge obstacle for practical applications. FE method must frequently consider complex manifold structures with many degrees of freedom (DOFs), which can easily become unsupportable for step-by-step frequency or time-domain analyses, in spite of technological developments in high-performance computer hardware and computer-aided engineering (CAE) software. When we consider topology optimization for complex manifold structures shown in Fig. 1, a large computation time would be required to calculate FE procedure with fine incremental frequencies or times.

One of the efficient and effective approaches to reduce the computation time in the FE procedure is reducing the system size prior to calculating the structural responses by using model reduction schemes. Many innovative model order reduction (MOR) methods, such as the Guyan reduction method [9,13], the mode superposition method (MS method) [22], the proper orthogonal decomposition method [20,27], the Ritz vector method (RV method) [15,22,26,28], the quasi-static Ritz vector method (QSRV method) [14,31], the multi-frequency quasi-static Ritz vector (MQSRV) method [30], and the transient quasi-static Ritz vector (TQSRV) method [31], have been developed. In [26], comparative transient dynamic analyses were performed using the load-dependent and the mode-superposition method based on the superposition of eigenvectors. In [8], they employed static recurrence procedures to generate the Ritz vectors. As such, these vector methods are best suited for low-frequency problems with the so-called quasi-static Ritz vector. In [3], the mode acceleration method and the mode superposition method have been employed to solve structural engineering problems. Especially, the time reduction effect of MOR methods come to remarkable when we have to deal with large scale problem [7]. Furthermore, MOR methods play an important role in connection to structural optimization, because many optimization and analysis iterations can be accelerated by a MOR approach in frequency domain [19,20,29,32]. The first MOR

* Corresponding author at: School of Mechanical Engineering, Hanyang University, Seoul, Republic of Korea.
E-mail address: ghy@hanyang.ac.kr (G.H. Yoon).

https://doi.org/10.1016/j.compstruc.2019.106146
0045-7949/

Fig. 1. Complex manifold structure.

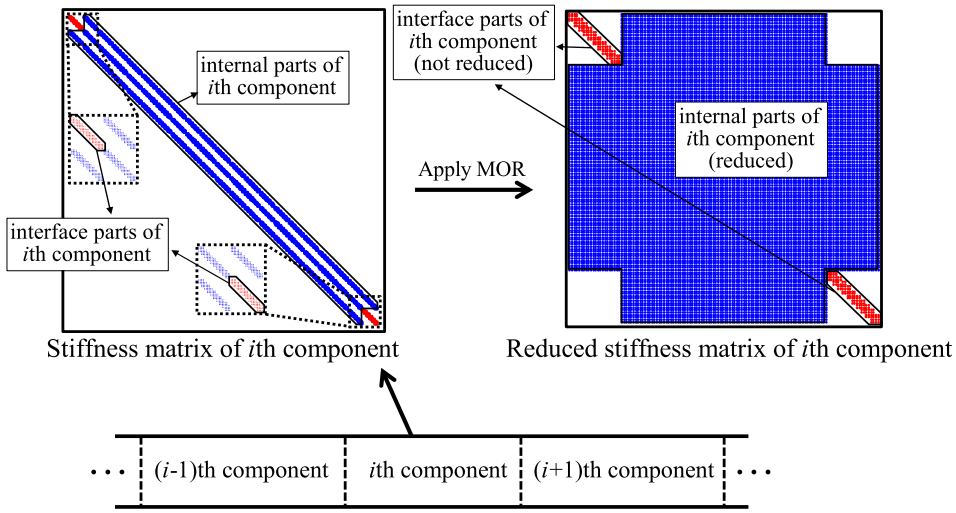

Fig. 2. Application of MMQSRV method in simple model.

approach in topology optimization can be found in [29] which investigated three types of MOR approaches, i.e., the MS, the RV, and the QSRV methods in topology optimization and showed that the mode superposition approach using the eigenvector can be troublesome due to the local mode issue. In [17], a MOR approach was applied to transient analysis in TO using the mode acceleration method (MAM) and mode displacement method (MDM). In [32,33], three kinds of objective functions (the mean dynamic compliance, the mean strain energy, and the mean squared displacement) were considered for TO. using MAM and MDM. Recently, Mediante et al. applied the projection-based parametric MOR method to reduce the computational cost of material or size optimization in large vibroacoustic models [21].

To contribute this research subject, the present study develops a new model order reduction for multiple components shown in Fig. 2. and applies it to the structural topology optimization with multiple components. To our best knowledge, the model order reductions for multiple components have been developed [4,12,18,20]. However, its application to structural topology optimization has not been studied or developed before this research. The existing model order reduction shows high efficiency with multi-components connected through points or shallow regions [18]. Indeed by presenting the model order reduction with Ritz vectors for multi-components connected through line or surface, the approximately structural responses are efficiently predicted. As the number of the Ritz vectors is proportional to the number of nodes along the interface lines, the numerical efficiency is also influenced. After that, its applications for efficient TO have been proposed.

The layout of the paper is organized as follows: First, we explain the basic concepts of density-based topology optimization and MR schemes. Then, a new MOR method called the multi-substructure multi-frequency quasi-static Ritz vector (MMQSRV) method for calculating the reduction bases for multiple substructures is presented. Using some analysis examples with arbitrary chosen material properties and boundary conditions, the efficiency and accuracy of the MMQSRV method will be checked. Then, the TO with the MMQSRV method will be solved. Finally, we summarize our findings and discuss some topics for future research in the conclusion.

2. Optimization formulation

2.1. Frequency response analysis of FE

Without the loss of generality, Newton's second equation is solved for the time-varying response of linear solid structure with time-varying force, $\mathbf{F}_t$ as follows:

$$\mathbf{M}\ddot{\mathbf{X}}_t + \mathbf{C}\dot{\mathbf{X}}_t + \mathbf{K}\mathbf{X}_t = \mathbf{F}_t, \tag{1}$$

where $\mathbf{M}$, $\mathbf{C}$, and $\mathbf{K}$ are the mass matrix, the damping matrix, and the stiffness matrix. The time-varying displacements, velocities, and accelerations of the structure are denoted by $\mathbf{X}_t$, $\dot{\mathbf{X}}_t$, and $\ddot{\mathbf{X}}_t$, respectively. For the sake of simplicity, it is assumed that the following Rayleigh damping with damping coefficients α_r and β_r in Eq. (2).

$$\mathbf{C} = \alpha_r\mathbf{M} + \beta_r\mathbf{K} \tag{2}$$

For the frequency response analysis, the following harmonic excitation is assumed [1].

$$\mathbf{X}_t = \mathbf{X}e^{i\omega t},\ \mathbf{F}_t = \mathbf{F}e^{i\omega t} \tag{3}$$

The dynamic stiffness matrix, **S**, can be derived as follows:

$$\mathbf{SX} = \mathbf{F}, \quad \mathbf{S} = -\omega^2\mathbf{M} + i\omega\mathbf{C} + \mathbf{K} \tag{4}$$

2.2. Statement of topology optimization formulation

Optimized design for given static or dynamic external loads has been an important issue in many structural applications. In this study, the topology optimization problem involves a volume constraint and strives to minimize the dynamic compliance defined by Ma et al. [19] and Jensen [11]. The topology optimization of a linear problem minimizing the dynamic compliance and subject to a volume constraint can be formulated as follows:

$$\begin{aligned} \underset{\gamma}{\text{Minimize}} \quad & \Phi = \int_{\omega_s}^{\omega_e} \left|\mathbf{F}^{\mathrm{T}}\mathbf{X}\right| d\omega \\ \text{Subject to} \quad & \sum_{i=1}^{NE} \gamma_i \mathrm{v}_i \leqslant \mathrm{V}^* \\ & \mathbf{M}\ddot{\mathbf{X}}_t + \mathbf{C}\dot{\mathbf{X}}_t + \mathbf{K}\mathbf{X}_t = \mathbf{F}_t \\ & 0 < \gamma \leqslant 1 \end{aligned} \tag{5}$$

where the starting and ending angular velocities are denoted by ω_s and ω_e, respectively. The design variable γ is varying from 0 to 1. The volume of the i-th element and the prescribed volume limit are v_i and V^*, respectively. To solve the optimization problem in (5), the method of moving asymptotes (MMA), is employed here. Meanwhile, for the sensitivity analysis for the objective function and the constraint with respect to design variable γ, the adjoint variable method (AVM) and Lagrange multiplier method are adopted. The sensitivity analysis is derived via the following:

$$\phi_L = \phi(\omega) + \lambda_1^{\mathrm{T}}(\mathbf{SX} - \mathbf{F}) + \lambda_2^{\mathrm{T}}(\bar{\mathbf{S}}\,\bar{\mathbf{X}} - \bar{\mathbf{F}}) \quad \text{where } \phi = \left|\mathbf{F}^{\mathrm{T}}\mathbf{X}\right| \tag{6}$$

The conjugate dynamic stiffness and the conjugate force are denoted by $\bar{\mathbf{S}}$ and $\bar{\mathbf{F}}$, respectively. The Lagrange multipliers are denoted by λ_1 and λ_2, respectively. By differentiating the Lagrange equation ϕ_L with respect to the design variable γ, the sensitivity analysis and two adjoint variables λ_1 and λ_2 can be obtained as follows:

$$\frac{d\phi_L}{d\gamma} = \frac{d\phi}{d\gamma} + \lambda_1^{\mathrm{T}}\left(\frac{\partial \mathbf{S}}{\partial\gamma}\mathbf{X} - \frac{\partial \mathbf{F}}{\partial\gamma}\right) + \lambda_2^{\mathrm{T}}\left(\frac{\partial \bar{\mathbf{S}}}{\partial\gamma}\bar{\mathbf{X}} - \frac{\partial \bar{\mathbf{F}}}{\partial\gamma}\right) \tag{7}$$

$$\mathbf{S}\lambda_1 = \frac{1}{2}\left(-\frac{\partial\phi}{\partial \mathbf{X}_{real}} + i\frac{\partial\phi}{\partial \mathbf{X}_{imag}}\right) \tag{8}$$

$$\begin{aligned} \bar{\mathbf{S}}\lambda_2 &= \frac{1}{2}\left(-\frac{\partial\phi}{\partial \mathbf{X}_{real}} - i\frac{\partial\phi}{\partial \mathbf{X}_{imag}}\right) \text{ or} \\ \bar{\mathbf{S}}\lambda_2 &= \frac{1}{2}\left(-\frac{\partial\phi}{\partial \mathbf{X}_{real}} + i\frac{\partial\phi}{\partial \mathbf{X}_{imag}}\right) \end{aligned} \tag{9}$$

Because Lagrange multipliers λ_1 and λ_2 are equal to each other, by comparing Eq. (10) with Eq. (11), we can simply get the following equation:

$$\frac{d\phi_L}{d\gamma} = \frac{\partial\phi}{\partial\gamma} + 2\mathrm{Real}\left(\lambda_1^{\mathrm{T}}\left(\frac{\partial \mathbf{S}}{\partial\gamma}\mathbf{X} - \frac{\partial \mathbf{F}}{\partial\gamma}\right)\right) \tag{10}$$

$$\mathbf{S}\lambda = -\frac{1}{2}\left(-\frac{\partial\phi}{\partial \mathbf{X}_{real}} - i\frac{\partial\phi}{\partial \mathbf{X}_{imag}}\right), \quad \lambda \equiv \lambda_1 = \bar{\lambda}_2 \tag{11}$$

Finally, the sensitivity value can be obtained as follows.

$$\frac{d\Phi}{d\gamma} = \int_{\omega_s}^{\omega_e} 2\mathrm{Real}\left(\lambda^{\mathrm{T}}\left(\frac{d\mathbf{S}}{\delta\gamma}\mathbf{X}\right)\right) d\omega \tag{12}$$

$$\lambda = \frac{-\alpha}{2}\mathbf{X},\ \alpha = \frac{\mathbf{X}^{\mathrm{T}}\mathbf{F}}{\left|\mathbf{X}^{\mathrm{T}}\mathbf{F}\right|}, \quad \lambda \equiv \lambda_1 = \bar{\lambda}_2 \tag{13}$$

3. Model reduction (MR) schemes for topology optimization

3.1. Introduction of model reduction schemes

For precise response calculation, the number of DOFs in a computational model is increased significantly over time. Therefore, the solutions of refined FE meshes are difficult for even the most advanced and state-of-the-art computational systems within a moderate computation time. In frequency response analysis, these limits are often overcome by applying a MOR scheme to reduce the size of the assembled stiffness and mass matrices. Many relevant studies have developed MOR methods, such as the Guyan reduction method [9,13], MS method [22], RV method [22,26,28], QSRV method [8], MQSRV method [30], TQSRV method [31], and proper orthogonal decomposition method [16]. By approximating the original structural response **X** with the reduced response $\boldsymbol{\Psi}\mathbf{Q}$, the size of the linear algebra system can be decreased by transforming a large set of system equations into a small set of equations [29,30]. From a mathematical point of view, the approximated response $\mathbf{X}_A$ of the original response **X** can be defined as follows:

$$\mathbf{AX} = \mathbf{B}, \tag{14}$$

$$\underbrace{\mathbf{X}}_{n_s\times 1} = \underbrace{\Psi}_{n_s\times n_d}\underbrace{\mathbf{Q}}_{n_d\times 1} + \underbrace{\mathbf{R}}_{n_s\times 1} \cong \underbrace{\Psi}_{n_s\times n_d}\underbrace{\mathbf{Q}}_{n_d\times 1} = \mathbf{X}_A, \tag{15}$$

$$\Psi = \left[\boldsymbol{\varphi}_1, \boldsymbol{\varphi}_2, \ldots, \boldsymbol{\varphi}_{n_d}\right] \quad (n_d \leqslant n_s), \tag{16}$$

where **A** and **B** denote an arbitrary $n_s \times n_s$ system matrix and an $n_s \times 1$ force vector, respectively; the number of DOFs in the system is denoted by n_s, and the number of reduced DOFs is denoted by n_d. In (15), the frequency-dependent basis vectors of the order n_d, the reduced unknown variables, and the residual matrix are denoted by Ψ, **Q**, and **R**, Respectively. By pre-multiplying Ψ^{T} into (14), the following reduced equation with order n_d is obtained.

$$\underbrace{\left\{\Psi^{\mathrm{T}}\mathbf{A}\Psi\right\}}_{n_d\times n_d}\underbrace{\mathbf{Q}}_{n_d\times 1} = \underbrace{\Psi^{\mathrm{T}}\mathbf{B}}_{n_d\times 1} \tag{17}$$

After solving this reduced system with order n_d for **Q**, the approximate solution $\mathbf{X}_A$ can be recovered using (15). Because we use a small size of matrix ($n_d \ll n_s$), the involved computational time can be reduced.

Similarly, Newton's second equation (1) can be formulated as following:

$$\Psi^{\mathrm{T}}\mathbf{M}\ddot{\mathbf{X}} + \Psi^{\mathrm{T}}\mathbf{C}\dot{\mathbf{X}} + \Psi^{\mathrm{T}}\mathbf{K}\mathbf{X} = \Psi^{\mathrm{T}}\mathbf{F} \tag{18}$$

$$\underbrace{\Psi^{\mathrm{T}}\mathbf{M}\Psi}_{\mathbf{M}_R}\ddot{\mathbf{Q}} + \underbrace{\Psi^{\mathrm{T}}\mathbf{C}\Psi}_{\mathbf{C}_R}\dot{\mathbf{Q}} + \underbrace{\Psi^{\mathrm{T}}\mathbf{K}\Psi}_{\mathbf{K}_R}\mathbf{Q} = \underbrace{\Psi^{\mathrm{T}}\mathbf{F}}_{\mathbf{F}_R} \tag{19}$$

Now the original system's displacement matrix **X** can be represented by recovering process as follows:

$$\mathbf{X} \cong \mathbf{X}_A = \Psi\mathbf{Q} \tag{20}$$

The sensitivity analysis with the solutions or the responses by the present MOR approach is similar to the previous one. In other words, the solutions in (6) and the following adjoint systems are simply replaced by the responses by the responses of the present MOR approach as follows:

$$\phi_L = \phi(\omega) + \lambda_1^{\mathrm{T}}(\mathbf{S}\mathbf{X}_{\mathrm{A}} - \mathbf{F}) + \lambda_2^{\mathrm{T}}(\bar{\mathbf{S}}\bar{\mathbf{X}}_{\mathrm{A}} - \bar{\mathbf{F}}) \quad \text{where } \phi = \left|\mathbf{F}^{\mathrm{T}}\mathbf{X}_{\mathrm{A}}\right| \tag{21}$$

$$\frac{d\Phi}{d\gamma} = \int_{\omega_s}^{\omega_e} 2\mathrm{Real}\left(\lambda^{\mathrm{T}}\frac{d\mathbf{S}}{\delta\gamma}\mathbf{X}_{\mathrm{A}}\right)d\omega, \quad \lambda = \frac{-\alpha}{2}\mathbf{X}_{\mathrm{A}},\ \alpha = \frac{\mathbf{X}_{\mathrm{A}}^{\mathrm{T}}\mathbf{F}}{\left|\mathbf{X}_{\mathrm{A}}^{\mathrm{T}}\mathbf{F}\right|}, \tag{22}$$

3.1.1. Multi-frequency quasi-static Ritz vector (MQSRV method)

The RV and QSRV methods construct their reduction bases Ψ by considering the external force **F**, the mass matrix **M**, and the stiffness matrix **K**. The order m Krylov subspace κ_m, generated by an arbitrary matrix **A** and an arbitrary vector **B**, is the linear subspace, as follows:

$$\kappa_m(\mathbf{A},\mathbf{B}) = \mathrm{span}\{\mathbf{B},\mathbf{A}\mathbf{B},\mathbf{A}^2\mathbf{B},\cdots,\mathbf{A}^{m-1}\mathbf{B}\} \tag{23}$$

For the practical computational implementation of the RV or QSRV method with the Krylov subspace in (23), the bases are stored through the following procedures.

$$\boldsymbol{\varphi}_1^* \equiv (\mathbf{K} - \omega_c^2\mathbf{M})^{-1}\mathbf{F} \quad (\text{LU decomposition}) \tag{24}$$

$$\boldsymbol{\varphi}_1 = \frac{1}{\sqrt{\boldsymbol{\varphi}_1^{*\mathrm{T}}\mathbf{M}\boldsymbol{\varphi}_1^*}}\boldsymbol{\varphi}_1^* \tag{25}$$

$$\text{Krylov subspace}: \boldsymbol{\varphi}_j^* \equiv (\mathbf{K} - \omega_c^2\mathbf{M})^{-1}(\mathbf{M}\boldsymbol{\varphi}_{j-1}) \quad (\text{LU decomposition}) \tag{26}$$

$$\text{Orthogonalization}: \boldsymbol{\varphi}_j^{**} \equiv \boldsymbol{\varphi}_j^* - \sum_{k=1}^{j-1}(\boldsymbol{\varphi}_k^{\mathrm{T}}\mathbf{M}\boldsymbol{\varphi}_j^*)\boldsymbol{\varphi}_k \tag{27}$$

$$\text{Normalization}: \boldsymbol{\varphi}_j = \frac{1}{\sqrt{\boldsymbol{\varphi}_j^{**\mathrm{T}}\mathbf{M}\boldsymbol{\varphi}_j^{**}}}\boldsymbol{\varphi}_j^{**} \tag{28}$$

where ω_c is the center angular velocity of interest. When $\omega_c = 0$, the QSRV and TQSRV methods become the RV method.

In addition, the MQSRV method was developed as an extension of the QSRV method. The MQSRV method adds the Krylov subspace bases constructed at multiple center frequencies to frequency-dependent systems, as follows:

$$\boldsymbol{\varphi}_{s,1} \equiv (\mathbf{K}(\omega_{c,s}) - \omega_{c,s}^2\mathbf{M}(\omega_{c,s}))^{-1}\mathbf{F}(\omega_{c,s}) \tag{29}$$

$$\boldsymbol{\varphi}_{s,j} \equiv (\mathbf{K}(\omega_{c,s}) - \omega_{c,s}^2\mathbf{M}(\omega_{c,s}))^{-1}(\mathbf{M}(\omega_{c,s})\boldsymbol{\varphi}_{s,j-1}), \tag{30}$$

$$\omega_{c,s} = \frac{\omega_{s,start} + \omega_{s,end}}{2}, \quad s = 1,\ldots,nf, \quad j = 1,\ldots,n_{d,s} \tag{31}$$

where the starting frequency, the ending frequency, and the center frequency of the s-th frequency domain are denoted by $\omega_{s,start}$, $\omega_{s,end}$, and $\omega_{c,s}$, respectively, and the total number of considered frequency domains is nf. The number of bases calculated for the s-th frequency domain is denoted by $n_{d,s}$. The following bases are then constructed for the MQSRV method:

$$\Psi = \left[\underbrace{\boldsymbol{\varphi}_{1,1}\cdots\boldsymbol{\varphi}_{1,n_{d,1}}}_{\text{the 1st domain}}, \underbrace{\boldsymbol{\varphi}_{1,2}\cdots\boldsymbol{\varphi}_{1,n_{d,2}}}_{\text{the 2nd domain}} \cdots \underbrace{\boldsymbol{\varphi}_{1,nf-1}\cdots\boldsymbol{\varphi}_{1,n_{d,nf-1}}}_{\text{the }(nf-1)\text{th domain}} \underbrace{\boldsymbol{\varphi}_{1,nf}\cdots\boldsymbol{\varphi}_{1,n_{d,nf}}}_{\text{the }(nf)\text{th domain}}\right], \tag{32}$$

where the mass orthogonalized bases of the MQSRV method for the i-th basis at the s-th center angular velocity are denoted by $\boldsymbol{\varphi}_{i,s}$. The number of bases at the s-th center angular velocity is denoted by $n_{d,s}$. After the bases of the QSRV method are built, the structural response **X** is again approximated.

$$\mathbf{X} \cong \mathbf{X}_A = \Psi\mathbf{Q} \tag{33}$$

One of the reasons to use those combined bases is that multi-frequency Krylov subspace bases effectively approximate the harmonic motion of a structural part in a wide range of frequency domains. The MQSRV method is thus effective for harmonic systems.

3.1.2. A new MOR method: multi-substructure multi-frequency quasi-static Ritz vector (MMQSRV)

Many novel MOR methods have been developed and implemented to accommodate the differences and uniqueness of various engineering applications. These efforts have been successfully adopted in open and commercial analysis software packages to accelerate solution procedures. However, because all these methods use internal information, easy access to internal information is essential. Therefore, confining our interest to structural analysis, the existing MOR models have the following issues and limitations.

Issue 1: It is impossible to use existing MOR methods for multiple-component systems with multiple subcomponents manufactured by different vendors who do not share their core analysis data, even with restrictions.

Issue 2: These existing MOR methods are commonly based on global stiffness and mass matrices. If some small parts of a system are modified, calculating and assembling new stiffness and mass matrices will be drawbacks of the existing MOR methods because they require additional computational resources, i.e., computing time.

As a new remedy for these structural problems, we present the MMQSRV method, a new MOR method that is applicable to multiple components and is based on the substructure method that uses the bases of the MQSRV method and TQSRV method. In this new MOR method, we divide a large computational system into several subcomponents and reduce the system matrices of each divided component using reduction bases. Therefore, the MMQSRV method offers the following advantages as solutions to the above issues.

Advantage 1: Because the basis calculation processes are achieved at the component level, each vendor is responsible for calculating its reduction bases without interacting with other components. A limitation of previous MOR method is that the meshes of multiple components should be continuous at the interfaces among subcomponents.

Advantage 2: Because the reduction processes are achieved at the component level, it is unnecessary to assemble or determine global stiffness and mass matrices for the mechanical system. The DOFs at the interfaces should be retained in the reduced systems.

Systematic calculation of reduction bases

To derive the reduction bases systematically for the MMQSRV method, we consider a mechanical system with multiple components. Some conventions should be defined, as follows:

* The interfacing node set (I_i^j): the nodes along the interfacing lines between i-th and j-th components.
* The interfacing element set: finite elements with at least one interfacing node.
* The adjacent interfacing node set (AI_i^j): the nodes composed of interfacing elements, excluding the interfacing nodes between i-th and j-th components.
* The adjacent interfacing node ($AIN_k^{(i,j)}$): the kth node of the adjacent interfacing node set AI_i^j.
* The number of adjacent interfacing nodes (in_i^j): the number of nodes in the adjacent interfacing node set AI_i^j.
* The internal node (I_i^i): the node set inside the i-th substructure, excluding the interfacing nodes of each substructure.

The following effective stiffness matrix is then decomposed as follows:

$$\mathbf{S}_j = -\omega^2 \boldsymbol{M}_j + i\omega \boldsymbol{C}_j + \boldsymbol{K}_j \tag{34}$$

$$\mathbf{S} = \sum_j \mathbf{S}_j \tag{35}$$

The stiffness matrix components can be represented as follows:

$$\mathbf{S}_i = \left[\begin{array}{ccc|c|cccc} \mathbf{S}_i^{I_1^i,I_1^i} & \cdots & \mathbf{0} & \mathbf{S}_i^{I_1^i,I_i^i} & & & & \\ \vdots & \ddots & \vdots & \vdots & & \mathbf{0} & & \\ \mathbf{0} & \cdots & \mathbf{S}_i^{I_{i-1}^i,I_{i-1}^i} & \mathbf{S}_i^{I_{i-1}^i,I_i^i} & & & & \\ \hline \mathbf{S}_i^{I_i^i,I_1^i} & \cdots & \mathbf{S}_i^{I_i^i,I_{i-1}^i} & \mathbf{S}_i^{I_i^i,I_i^i} & \mathbf{S}_i^{I_i^i,I_{i+1}^i} & \cdots & \mathbf{S}_i^{I_i^i,I_n^i} \\ \hline & & & \mathbf{S}_i^{I_{i+1}^i,I_i^i} & \mathbf{S}_i^{I_{i+1}^i,I_{i+1}^i} & & \mathbf{0} & \\ & \mathbf{0} & & \vdots & & \ddots & & \\ & & & \mathbf{S}_i^{I_n^i,I_i^i} & \mathbf{0} & & \mathbf{S}_i^{I_n^i,I_n^i} & \end{array}\right], \tag{36}$$

where the symmetric stiffness matrix of the i-th component is $\mathbf{S}_i$, which can be decomposed by the values along the kth interfacing node set, i.e., $\mathbf{S}_i^{I_k^i,I_k^i}$ and $\mathbf{S}_i^{I_k^i,I_i^i}$. Without the loss of generality, the i-th internal DOFs ($\mathbf{S}_i^{I_i^i,I_i^i}$) can be condensed and the whole system matrix can be written as follows:

$$\mathbf{S}_i^R = \left[\begin{array}{ccc|c|cccc} \mathbf{S}_i^{I_1^i,I_1^i} & \cdots & \mathbf{0} & \mathbf{S}_i^{I_1^i,I_i^i}\boldsymbol{\varphi}_i & & & & \\ \vdots & \ddots & \vdots & \vdots & & \mathbf{0} & & \\ \mathbf{0} & \cdots & \mathbf{S}_i^{I_{i-1}^i,I_{i-1}^i} & \mathbf{S}_i^{I_{i-1}^i,I_i^i}\boldsymbol{\varphi}_i & & & & \\ \hline \boldsymbol{\varphi}_i^{\mathrm{T}}\mathbf{S}_i^{I_i^i,I_1^i} & \cdots & \boldsymbol{\varphi}_i^{\mathrm{T}}\mathbf{S}_i^{I_i^i,I_{i-1}^i} & \boldsymbol{\varphi}_i^{\mathrm{T}}\mathbf{S}_i^{I_i^i,I_i^i}\boldsymbol{\varphi}_i & \boldsymbol{\varphi}_i^{\mathrm{T}}\mathbf{S}_i^{I_i^i,I_{i+1}^i} & \cdots & \boldsymbol{\varphi}_i^{\mathrm{T}}\mathbf{S}_i^{I_i^i,I_n^i} \\ \hline & & & \mathbf{S}_i^{I_{i+1}^i,I_i^i}\boldsymbol{\varphi}_i & \mathbf{S}_i^{I_{i+1}^i,I_{i+1}^i} & & \mathbf{0} & \\ & \mathbf{0} & & \vdots & & \ddots & & \\ & & & \mathbf{S}_i^{I_n^i,I_i^i}\boldsymbol{\varphi}_i & \mathbf{0} & & \mathbf{S}_i^{I_n^i,I_n^i} & \end{array}\right] \tag{37}$$

Depending on the choice of MOR scheme, many different characteristics appear for $\mathbf{S}_i^R$. In this study, we use the MQSRV method with some Krylov subspace for $\boldsymbol{\varphi}_i$. However, it is unclear how to compute the Krylov subspaces for each internal component because some non-zero external forces and the full-rank system stiffness matrices are essential, and they often do not exist. To resolve this vector space issue, our proposed approach introduces a pseudo-fixed boundary along the interfacing node set and some pseudo-forces at the adjacent interfacing node set.

This research calculates the bases using the MQSRV approach. Each component is considered as an independent mechanical system that interacts with adjacent components. How to compute the Krylov subspace of each component becomes a critical issue because some external forces and the system stiffness matrices are required, and often some substructures are missing external forces and constraints. Therefore, it is regarded that the mechanically interacting forces among substructures as external forces for each component. Mathematically, the stiffness matrices of adjacent substructures directly influence the motions of the internal nodes of each substructure through the interfacing nodes, as shown in Fig. 3. One limitation is that matching discretization among substructures should be used, as shown in Fig. 3; therefore, with non-matching discretization, the proposed approach cannot be applied. All the nodes constructing the FE adjacent to the interface line, except those at the interface line, are of interest.

Fig. 3(a) is a schematic diagram of the interface. Some artificial point loads are applied to the DOFs of the adjacent interfacing node set, as shown in Fig. 3(b) for the multi-frequency Krylov subspaces. After that, it is possible to reduce the size of the system matrix using the MOR scheme.

The basis for the i-th substructure can then be written as follows:

$$\boldsymbol{\varphi}_i = \left[\begin{array}{c|c} \underbrace{\boldsymbol{\varphi}_i^{\text{external loads}}}_{\substack{\text{Bases for extanal loads}\\ \text{at the internal nodes of}\\ \text{the } i\text{th component } (I_i^i)}} & \underbrace{\boldsymbol{\varphi}_i^{\text{pseudo loads}}}_{\substack{\text{Bases for pseudo loads at}\\ \text{the adjacent interfacing nodes}\\ \text{of the } i\text{th component}}} \end{array}\right], \tag{38}$$

where the reduction bases of the i-th component are expressed as Eq. (38), comprising the bases for external loads and the bases for pseudo-loads. The bases for the external loads are calculated using external loads on the i-th component, if they exist. The reduction bases for the pseudo-loads are decomposed as follows:

$$\boldsymbol{\varphi}_i^{\text{pseudo loads}} = \left[\boldsymbol{\varphi}_i^{AI_i^1}, \boldsymbol{\varphi}_i^{AI_i^2}, \cdots, \boldsymbol{\varphi}_i^{AI_i^{i-1}}, \boldsymbol{\varphi}_i^{AI_i^{i+1}}, \cdots, \boldsymbol{\varphi}_i^{AI_i^n}\right] \tag{39}$$

$$\boldsymbol{\varphi}_i^{AI_i^j} = \left[\left[\boldsymbol{\varphi}_i^{AIN_1^{(i,j)}}, \boldsymbol{\varphi}_i^{AIN_2^{(i,j)}}, \cdots, \boldsymbol{\varphi}_i^{AIN_{in_i^j}^{(i,j)}}\right]_x, \left[\boldsymbol{\varphi}_i^{AIN_1^{(i,j)}}, \boldsymbol{\varphi}_i^{AIN_2^{(i,j)}}, \cdots, \boldsymbol{\varphi}_i^{AIN_{in_i^j}^{(i,j)}}\right]_y\right], \tag{40}$$

where the reduction bases of the i-th component along the j-th adjacent interface node are denoted by $\boldsymbol{\varphi}_i^{AI_i^j}$. As the number of bases increases, the accuracy is improved but the computation time is also increased.

3.1.3. Calculation of reduction bases example: Simple 2-component cantilever problem

To understand the MMQSRV method, let us consider the system in Fig. 4 with the predefined notations.

The effective system matrix can be written as follows:

$$\left[\begin{array}{ccc} \mathbf{S}_1^{I_1^1,I_1^1} & \mathbf{S}_1^{I_1^1,I_1^2} & \mathbf{0} \\ \mathbf{S}_1^{I_1^2,I_1^1} & \mathbf{S}_1^{I_1^2,I_1^2}+\mathbf{S}_2^{I_1^2,I_1^2} & \mathbf{S}_2^{I_1^2,I_2^2} \\ \mathbf{0} & \mathbf{S}_2^{I_2^2,I_1^2} & \mathbf{S}_2^{I_2^2,I_2^2} \end{array}\right]\left[\begin{array}{c} \mathbf{X}_1^{I_1^1} \\ \mathbf{X}_1^{I_1^2} \\ \mathbf{X}_2^{I_2^2} \end{array}\right] = \left[\begin{array}{c} \mathbf{F}_1^{I_1^1} \\ \mathbf{F}_1^{I_1^2} \\ \mathbf{F}_2^{I_2^2} \end{array}\right], \tag{41}$$

where the displacements of each node set are denoted by $\mathbf{X}_i^{I_i^j}$ (i, j = 1 or 2). The effective force vector is divided similarly. Without the loss of generality, the stiffness components corresponding to the DOFs of each node set are defined by $\mathbf{S}_m^{I_j^i,I_l^k}$ (i, j, k, l, m = 1 or 2). Before reducing the above system matrix, the reduction bases are generated independently for the first and second components.

The reduction bases $\boldsymbol{\varphi}_1$ are then computed via the following procedure.

$$\boldsymbol{\varphi}_1 = \left[\boldsymbol{\varphi}_1^{\text{external loads}},\ \boldsymbol{\varphi}_1^{\text{pseudo loads}}\right] \tag{42}$$

Because the first component has an external load, the temporary bases for the external load before normalization and orthogonalization are computed using the following procedure.

$$\begin{aligned} \tilde{\boldsymbol{\varphi}}_1^{\text{external loads}} &= \tilde{\boldsymbol{\varphi}}_1^{I_1^1} \\ &= \left[\overbrace{(\tilde{\boldsymbol{\varphi}}_{(1,1),1}^{I_1^1}, \cdots, \tilde{\boldsymbol{\varphi}}_{(n_{d,1},1),1}^{I_1^1})}^{\omega_{c,1}^{(1,1)}}, \cdots, \overbrace{(\tilde{\boldsymbol{\varphi}}_{(1,nf_{(e)}^{(1,1)}),1}^{I_1^1}, \cdots, \tilde{\boldsymbol{\varphi}}_{(n_{d,nf_{(e)}^{(1,1)}},nf_{(e)}^{(1,1)}),1}^{I_1^1})}^{\omega_{c,nf_{(e)}^{(1,1)}}^{(1,1)}}\right] \end{aligned} \tag{43}$$

$$\tilde{\boldsymbol{\varphi}}_{(1,m),1}^{I_1^1} = \left[\mathbf{K}_1^{I_1^1} - (\omega_{c,m}^{(1,1)})^2 \mathbf{M}_1^{I_1^1}\right]^{-1} \mathbf{F}^{I_1^1}, \quad (m = 1, \cdots, nf_{(e)}^{(1,1)}) \tag{44}$$

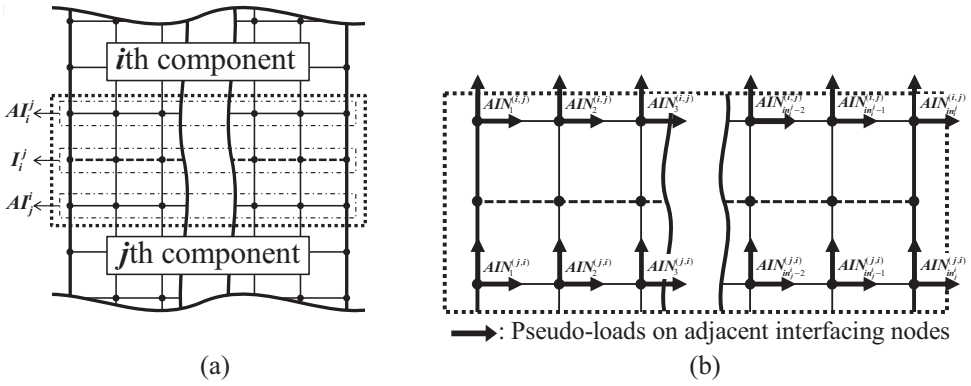

Fig. 3. Schematic diagram of an interface between two substructures.

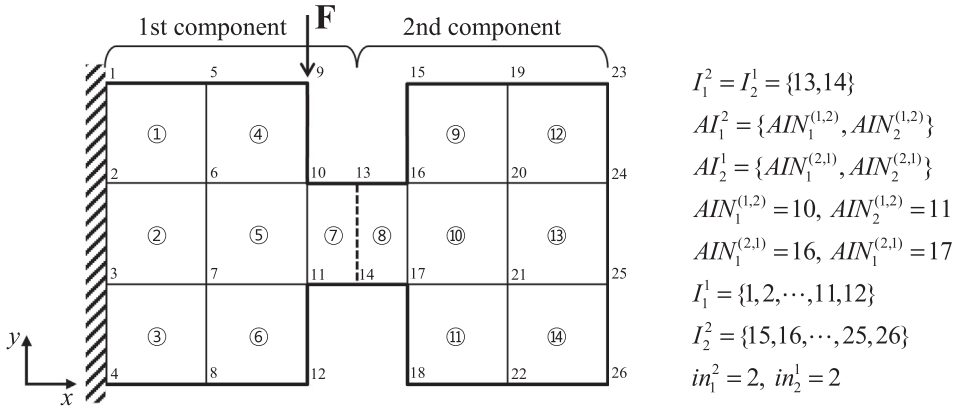

Fig. 4. An illustrative example with two substructures.

$$\overset{\sim}{\boldsymbol{\varphi}}{}^{I_1^1}_{(s,m),1} = \left[\mathbf{K}_1^{I_1^1} - (\omega_{c,m}^{(1,1)})^2\mathbf{M}_1^{I_1^1}\right]^{-1}\left[\mathbf{M}_1^{I_1^1}\overset{\sim}{\boldsymbol{\varphi}}{}^{I_1^1}_{(s-1,m),1}\right], \quad (s = 2,\cdots,n_{d,m}) \tag{45}$$

Furthermore, the reduction bases for three pseudo-loads at the first component are generated as in equations (46)–(50).

$$\begin{aligned}\overset{\sim}{\boldsymbol{\varphi}}{}_1^{\text{pseudo loads}} &= \overset{\sim}{\boldsymbol{\varphi}}{}_1^{AI_1^2} \\ &= \left[\overset{\sim}{\boldsymbol{\varphi}}{}_1^{\overbrace{AIN_1^{(1,2)}}^{10\text{th node}}}, \overset{\sim}{\boldsymbol{\varphi}}{}_1^{\overbrace{AIN_2^{(1,2)}}^{11\text{th node}}}\right] \text{(Unit pseudo - loads applied.)}\end{aligned} \tag{46}$$

$$\overset{\sim}{\boldsymbol{\varphi}}{}_1^{AIN_k^{(1,2)}} = \left[\overset{\sim}{\boldsymbol{\varphi}}{}_{1,x}^{AIN_k^{(1,2)}}, \overset{\sim}{\boldsymbol{\varphi}}{}_{1,y}^{AIN_k^{(1,2)}}\right], \quad (k = 1,2), \tag{47}$$

$$\overset{\sim}{\boldsymbol{\varphi}}{}_{1,x}^{AIN_k^{(1,2)}} = \left[\overbrace{(\overset{\sim}{\boldsymbol{\varphi}}{}_{(1,1),1,x}^{AIN_k^{(1,2)}},\cdots,\overset{\sim}{\boldsymbol{\varphi}}{}_{(n_{d,1},1),1,x}^{AIN_k^{(1,2)}})}^{\omega_{c,1}^{(1,1)}},\cdots,\overbrace{(\overset{\sim}{\boldsymbol{\varphi}}{}_{(1,nf_{(\text{p})}^{(1,2)}),1,x}^{AIN_k^{(1,2)}},\cdots,\overset{\sim}{\boldsymbol{\varphi}}{}_{(n_{d,nf_{(\text{p})}^{(1,2)}},nf_{(\text{p})}^{(1,2)}),1,x}^{AIN_k^{(1,2)}})}^{\omega_{c,nf_{(\text{p})}^{(1,2)}}^{(1,1)}}\right], \tag{48}$$

$$\overset{\sim}{\boldsymbol{\varphi}}{}_{(1,m),1,x}^{AIN_k^{(1,2)}} = \left[\mathbf{K}_1^{I_1^1} - (\omega_{c,m}^{(1,1)})^2\mathbf{M}_1^{I_1^1}\right]^{-1}\mathbf{F}_x^{AIN_k^{(1,2)}}, \quad (m = 1,\cdots,nf_{(\text{p})}^{(1,2)}) \tag{49}$$

$$\overset{\sim}{\boldsymbol{\varphi}}{}_{(s,m),1,x}^{AIN_k^{(1,2)}} = \left[\mathbf{K}_1^{I_1^1} - (\omega_{c,m}^{(1,1)})^2\mathbf{M}_1^{I_1^1}\right]^{-1}\left[\mathbf{M}_1^{I_1^1}\overset{\sim}{\boldsymbol{\varphi}}{}_{(s-1,m),1,x}^{AIN_k^{(1,2)}}\right], \quad (s = 2,\cdots,n_{d,m}) \tag{50}$$

where $nf_{(\text{p})}^{(1,2)}$ is the number of center frequencies for the pseudo-loads ($\mathbf{F}^{AI_1^2}$), and $n_{d,m}$ is the number of Krylov subspaces at the m-th center frequency ($\omega_{c,m}^{(1,1)}$) for pseudo-loads ($\mathbf{F}^{AI_1^2}$). The orthogonalization and normalization processes are applied to the temporary bases $\overset{\sim}{\boldsymbol{\varphi}}{}_1^{\text{external loads}}$ and $\overset{\sim}{\boldsymbol{\varphi}}{}_1^{\text{pseudo loads}}$ for $\boldsymbol{\varphi}_1^{\text{external loads}}$ and $\boldsymbol{\varphi}_1^{\text{pseudo loads}}$, respectively.

The reduction bases $\boldsymbol{\varphi}_2$ are computed using the following procedure.

$$\boldsymbol{\varphi}_2 = \left[\boldsymbol{\varphi}_2^{\text{external loads}},\ \boldsymbol{\varphi}_2^{\text{pseudo loads}}\right] \tag{51}$$

Because the second component has no external load, the bases for external load are empty.

$$\boldsymbol{\varphi}_2^{\text{external loads}} = [\text{Empty}] \tag{52}$$

Therefore, only the temporary reduction bases from the pseudo-loads exist.

$$\begin{aligned}\overset{\sim}{\boldsymbol{\varphi}}{}_2^{\text{pseudo loads}} &= \overset{\sim}{\boldsymbol{\varphi}}{}_2^{AI_2^1} \\ &= \left[\overset{\sim}{\boldsymbol{\varphi}}{}_2^{\overbrace{AIN_1^{(2,1)}}^{16\text{th node}}}, \overset{\sim}{\boldsymbol{\varphi}}{}_2^{\overbrace{AIN_2^{(2,1)}}^{17\text{th node}}}\right] \text{(Unit pseudo - loads applied.)}\end{aligned} \tag{53}$$

$$\overset{\sim}{\boldsymbol{\varphi}}{}_2^{AIN_k^{(2,1)}} = \left[\overset{\sim}{\boldsymbol{\varphi}}{}_{2,x}^{AIN_k^{(2,1)}}, \overset{\sim}{\boldsymbol{\varphi}}{}_{2,y}^{AIN_k^{(2,1)}}\right], \quad (k = 1,2) \tag{54}$$

$$\overset{\sim}{\boldsymbol{\varphi}}{}_{2,x}^{AIN_k^{(2,1)}} = \left[\overbrace{(\overset{\sim}{\boldsymbol{\varphi}}{}_{(1,1),2,x}^{AIN_k^{(2,1)}},\cdots,\overset{\sim}{\boldsymbol{\varphi}}{}_{(n_{d,1},1),2,x}^{AIN_k^{(2,1)}})}^{\omega_{c,1}^{(2,2)}},\cdots,\overbrace{(\overset{\sim}{\boldsymbol{\varphi}}{}_{(1,nf_{(\text{p})}^{(2,1)}),2,x}^{AIN_k^{(2,1)}},\cdots,\overset{\sim}{\boldsymbol{\varphi}}{}_{(n_{d,nf_{(\text{p})}^{(2,1)}},nf_{(\text{p})}^{(2,1)}),2,x}^{AIN_k^{(2,1)}})}^{\omega_{c,nf_{(\text{p})}^{(2,1)}}^{(2,2)}}\right] \tag{55}$$

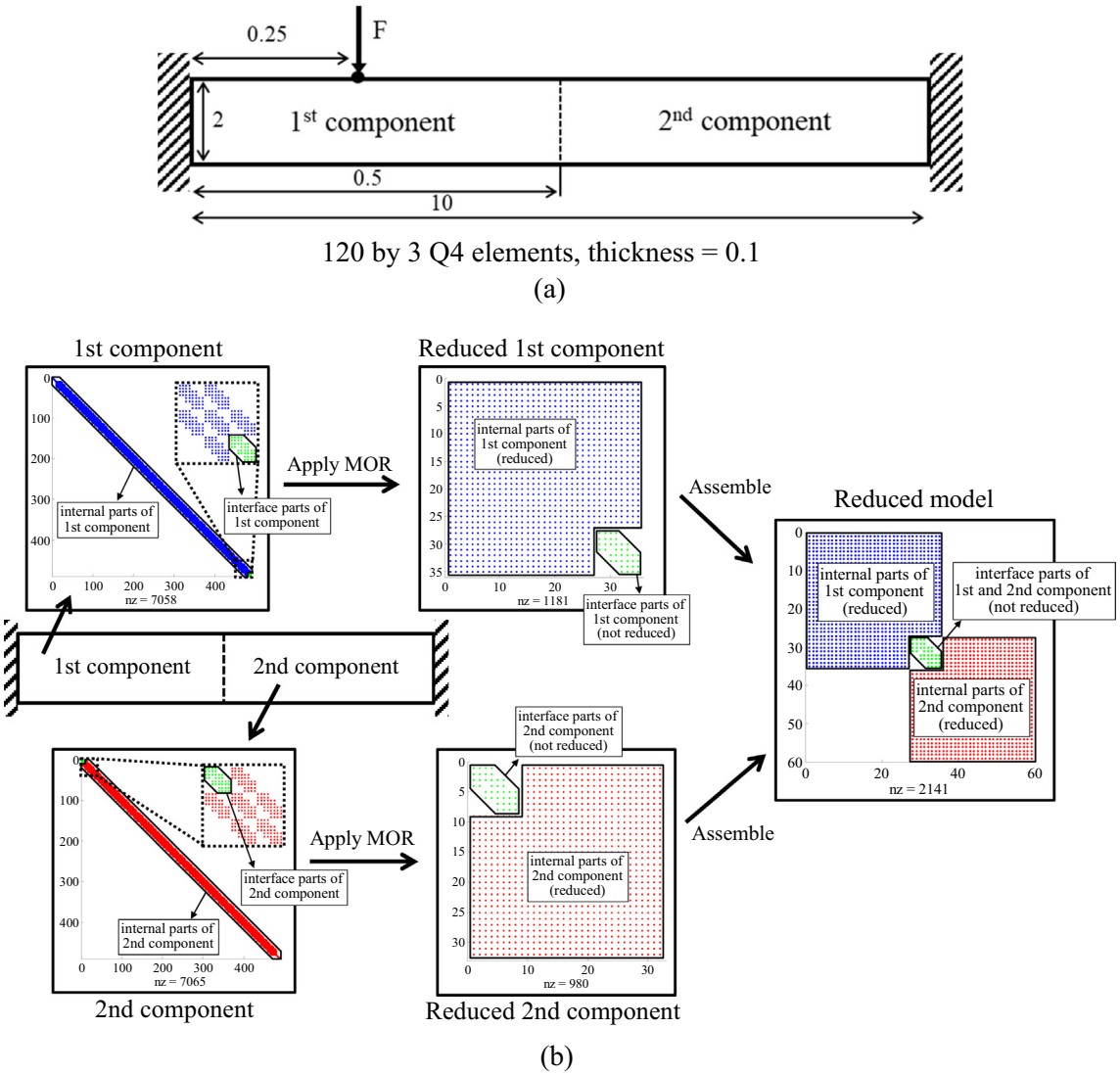

Fig. 5. Two-dimensional beam model with a point load (a) cantilever beam (120 × 3 linear Q4 elements) with the two subcomponents and (b) the reduction process for each model.

$$\tilde{\boldsymbol{\varphi}}^{AIN_k^{(2,1)}}_{(1,m),2,x} = \left[\mathbf{K}_2^{I_2^2} - \left(\omega_{c,m}^{(2,2)}\right)^2 \mathbf{M}_2^{I_2^2}\right]^{-1} \mathbf{F}_x^{AIN_k^{(2,1)}}, (m = 1, \cdots, nf_{(\mathrm{p})}^{(2,1)}) \tag{56}$$

$$\tilde{\boldsymbol{\varphi}}^{AIN_k^{(2,1)}}_{(s,m),2,x} = \left[\mathbf{K}_2^{I_2^2} - \left(\omega_{c,m}^{(2,2)}\right)^2 \mathbf{M}_2^{I_2^2}\right] \left[\mathbf{M}_2^{I_2^2} \tilde{\boldsymbol{\varphi}}^{AIN_k^{(2,1)}}_{(s-1,m),2,x}\right], (s = 2, \cdots, n_{d,m}) \tag{57}$$

where $nf_{(\mathrm{p})}^{(2,1)}$ is the number of center frequencies for pseudo-loads ($\mathbf{F}^{AI_2^1}$), and $n_{d,m}$ is the number of Krylov subspaces at the m-th center frequency ($\omega_{c,m}^{(2,2)}$) for pseudo-loads ($\mathbf{F}^{AI_2^1}$). After the above procedures, the orthogonalization and normalization processes are applied to the temporary bases $\tilde{\boldsymbol{\varphi}}_2^{\text{pseudo loads}}$ for $\boldsymbol{\varphi}_2^{\text{pseudo loads}}$.

Without loss of generality, we reduce the second subsystem before the first subsystem. The second component is first reduced with the reduction bases $\boldsymbol{\varphi}_2$, as follows:

$$\mathbf{X}^{I_2^2} \simeq \boldsymbol{\varphi}_2 \mathbf{Q}^{I_2^2} \tag{58}$$

The system matrix in Eq. (41) is then redefined as follows:

$$\begin{bmatrix} \mathbf{S}_1^{I_1^1,I_1^1} & \mathbf{S}_1^{I_1^1,I_1^2} & \mathbf{0} \\ \mathbf{S}_1^{I_1^2,I_1^1} & \mathbf{S}_1^{I_1^2,I_1^2} + \mathbf{S}_2^{I_1^2,I_1^2} & \mathbf{S}_2^{I_1^2,I_2^2}\boldsymbol{\varphi}_2 \\ \mathbf{0} & \boldsymbol{\varphi}_2^{\mathrm{T}}\mathbf{S}_2^{I_2^2,I_1^2} & \boldsymbol{\varphi}_2^{\mathrm{T}}\mathbf{S}_2^{I_2^2,I_2^2}\boldsymbol{\varphi}_2 \end{bmatrix} \begin{bmatrix} \mathbf{X}^{I_1^1} \\ \mathbf{X}^{I_1^2} \\ \mathbf{Q}^{I_2^2} \end{bmatrix} = \begin{bmatrix} \mathbf{F}^{I_1^1} \\ \mathbf{F}^{I_1^2} \\ \boldsymbol{\varphi}_2^{\mathrm{T}}\mathbf{F}^{I_2^2} \end{bmatrix} \quad \text{(The second component is reduced.)} \tag{59}$$

After the procedures from equations (53)–(57), we further reduce the system using the MMQSRV method for the first component, as follows:

$$\mathbf{X}^{I_1^1} \simeq \boldsymbol{\varphi}_1 \mathbf{Q}^{I_1^1} \tag{60}$$

By replacing $\mathbf{X}^{I_1^1}$ with $\boldsymbol{\varphi}_1\mathbf{Q}^{I_1^1}$, the system matrix is redefined as follows:

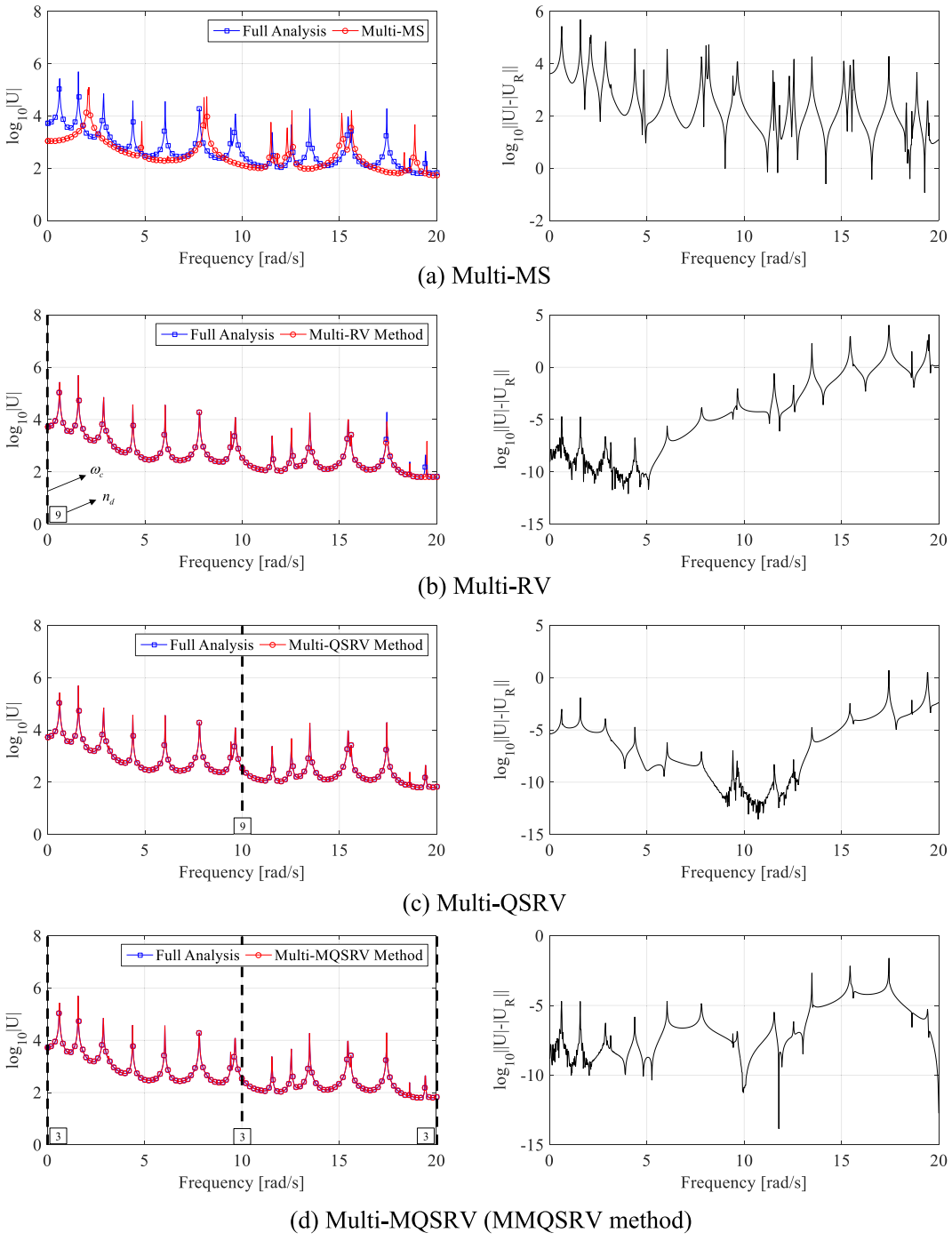

Fig. 6. FRF responses with (a) Multi-MS, (b) Multi-RV, (c) Multi-QSRV, and (d) Multi-MMQSRV methods.

Table 1
Computational speedup for MOR example (Fig. 6).

Number of degrees of freedom (1st component, 2nd component)	Multi-MS	Multi-RV	Multi-QSRV	MMQSRV
Center frequency (rad/s)	none	0	10	0, 10, 20
Computed number of bases at each center frequency	117 (60, 57) (eigen-modes)	9	9	3
Total number of bases (1st component, 2nd component)	117 (60, 57)			
Full finite element analysis	3.9286 s			
MMQSRV analysis (base generation, FRF analysis)	0.5128 s (0.1487 s, 0.3641 s)	0.4416 s (0.0461 s, 0.3955 s)	0.4216 s (0.0511 s, 0.3705 s)	0.4441 s (0.0719 s, 0.3722 s)
Speedup	7.6611	8.8963	9.3183	8.8462
Error indicator	1.0493	1.3923×10^{-2}	1.1197×10^{-5}	2.5231×10^{-8}

Table 2
The error indicator with respect to the number of Ritz vectors.

Number of Ritz vector	1	2	3	4	5	10
Error indicator	3.9033	5.6963×10^{-2}	2.5231×10^{-8}	6.7343×10^{-11}	5.8035×10^{-11}	6.3232×10^{-11}

$$\begin{bmatrix} \boldsymbol{\varphi}_1^{\mathrm{T}}\mathbf{S}_1^{I_1^1,I_1^1}\boldsymbol{\varphi}_1 & \boldsymbol{\varphi}_1^{\mathrm{T}}\mathbf{S}_1^{I_1^1,I_1^2} & \mathbf{0} \\ \mathbf{S}_1^{I_1^2,I_1^1}\boldsymbol{\varphi}_1 & \mathbf{S}_1^{I_1^2,I_1^2}+\mathbf{S}_2^{I_1^2,I_1^2} & \mathbf{S}_2^{I_1^2,I_2^2}\boldsymbol{\varphi}_2 \\ \mathbf{0} & \boldsymbol{\varphi}_2^{\mathrm{T}}\mathbf{S}_2^{I_2^2,I_1^2} & \boldsymbol{\varphi}_2^{\mathrm{T}}\mathbf{S}_2^{I_2^2,I_2^2}\boldsymbol{\varphi}_2 \end{bmatrix} \begin{bmatrix} \mathbf{Q}^{I_1^1} \\ \mathbf{X}^{I_1^2} \\ \mathbf{Q}^{I_2^2} \end{bmatrix} = \begin{bmatrix} \boldsymbol{\varphi}_1^{\mathrm{T}}\mathbf{F}^{I_1^1} \\ \mathbf{F}^{I_1^2} \\ \boldsymbol{\varphi}_2^{\mathrm{T}}\mathbf{F}^{I_2^2} \end{bmatrix} \quad \text{(The first component is reduced.)} \tag{61}$$

After all the above procedures, the DOFs of each subcomponent can be reduced, and efficient FE simulations are achievable. The next section provides several numerical examples to show the versatility and effectiveness of our MMQSRV approach.

It is crucial to have accurate finite element solutions to be incorporated with TO with the model order reduction. This research has concerned about not only the accuracy of the response of the finite element simulation but also the similarity of the optimal layouts with and without the model order reduction approach. To improve the accuracy of the solution, a proper model order reduction should be employed and the number of the bases of the model order reduction should be increased appropriately. In our numerical tests, we set, increase or decreases the number of the bases of the MMQSRV method to have the same optimization results as well as to get a higher speedup. For an example, it is possible to adopt the following norm-based error indicator to evaluate the accuracy of the finite element method with the MMQSRV method.

$$\text{Error indicator} = \frac{\int_{\omega_s}^{\omega_e} |\mathbf{X} - \mathbf{X}_{\mathrm{A}}| d\omega}{\int_{\omega_s}^{\omega_e} |\mathbf{X}| d\omega} \tag{62}$$

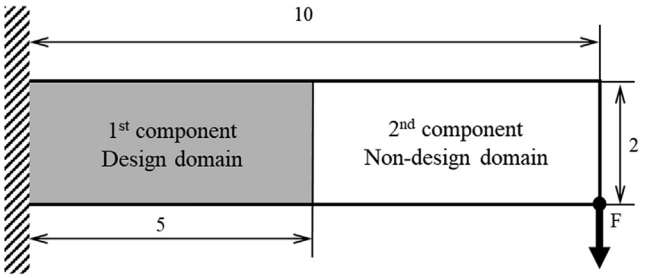

Fig. 8. Two-dimensional cantilever beam model (120 × 20 Q4 elements, ν=0.3, ρ=1, thickness = 1) with two subcomponents.

3.1.4. Comparison of model reduction methods

In this example, the two-dimensional beam structure in Fig. 5 (a) with two components is considered. The analysis domain with the two subcomponents is discretized into linear Q4 FE with 968 DOFs. The first and second subcomponents are connected through an interface line 0.1 m in height (marked by the dotted lines in Fig. 5(a)). The external point load is applied at the top-middle of the first component; the following results and conclusions from the MMQSRV method are unrelated to the loading conditions. Fig. 5(b) shows the overall MMQSRV procedure focusing on the stiffness matrices. The MMQSRV method excludes the stiffness sub-matrix for each component and preserves the interface information of the two components. After that, we compare the frequency response curves of the full FE model and the reduced

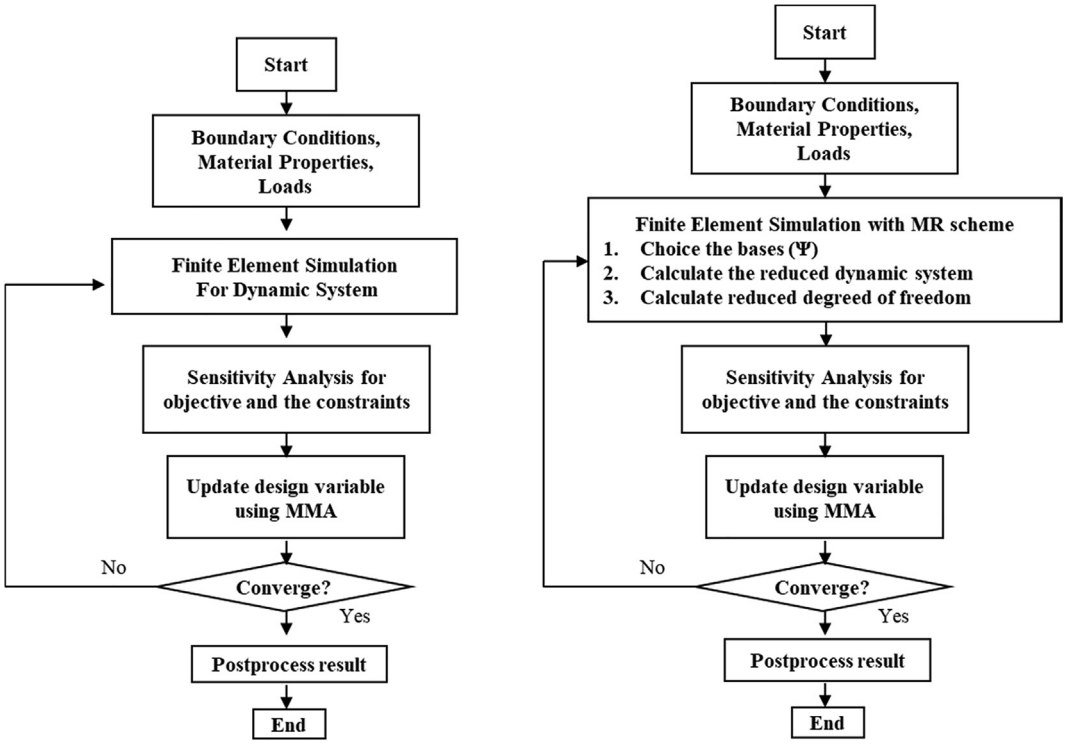

Fig. 7. Overview of topology optimization process without (left) and with (right) MR scheme.

model comparing the efficiency of the MMQSRV method with that of the original FE procedure.

To illustrate the effectiveness and properties of the MMQSRV method compared with those of the MS, RV, QSRV, and MQSRV methods, we consider the FE model shown in Fig. 5(a). The Young's modulus, density, and Poisson's ratio are set to 1 Pa, 1 kg/m^3, and 0.3, respectively. The analysis domain is discretized into 360 Q4 elements, and the number of DOFs is 968. The reduction bases from the MS, RV, and QSRV methods are employed in order to compare the efficiencies of these approaches to our present method. We then set the total number bases to be the same for a fair comparison at 117 bases (60 bases for the 1st component and 57 bases for the 2nd component). For the MS method, we use the eigenmodes of each component. For the RV, QSRV, and MMQSRV methods, the pseudo-forces to the adjacent nodes with either 0 rad/s (RV) or 10 rad/s (QSRV and MMQSRV) as the center frequency are added. To distinguish the previous MOR methods, we simply name them Multi-MS, Multi-RV, Multi-QSRV, and Multi-MQSRV (MMQSRV) methods. The analysis results are shown in Fig. 6. This example shows that the responses from the Multi-MS method are not accurate. Because of the adjacent interface and external components, it is difficult to construct the bases with the eigenvectors of one component. By contrast, the responses from the Multi-RV method are more accurate than those from the Multi-MS method near 0 rad/s. In the Multi-RV method, 9 bases are computed for the external load, and an additional 9 bases are computed for the pseudo-forces at the adjacent nodes. Among the tested methods, the Multi-MQSRV method shows the best accuracy. Because both MOR method uses the same number of bases, the total computation time is quite similar. The detailed analysis results are illustrated in Fig. 6 and Table 1. The error of MMQSRV method can be simply reduced by calculating Ritz vector using Krylov subspaces. Relation between the error and the number of Ritz vector is denoted in Table 2. In our numerical tests, errors less than 5 percent with more than 3 Ritz vectors can be achievable and the optimal layouts become similar to the solution without the model order reduction. The error may be increased with the existences of resonances; this feature will be detailly discussed in the numerical section.

4. Topology optimization examples

To show and compare the effectiveness of the MR schemes, several numerical examples are considered in this section. For the material interpolation, several approaches have been developed. Several interpolation approaches are available (See [5,6] for the level approach and references therein). In the present study, the SIMP (Solid Isotropic Material with Penalization) is employed. The finite element and the optimization procedures are implemented in the MATLAB framework. The design domains and material properties are arbitrarily chosen to show the potential of the MR schemes in topology optimization. For the convergence criteria of the optimization process, the following absolute change of objective values of two sequential optimization iterations are considered and the maximum optimization iteration is set to 100.

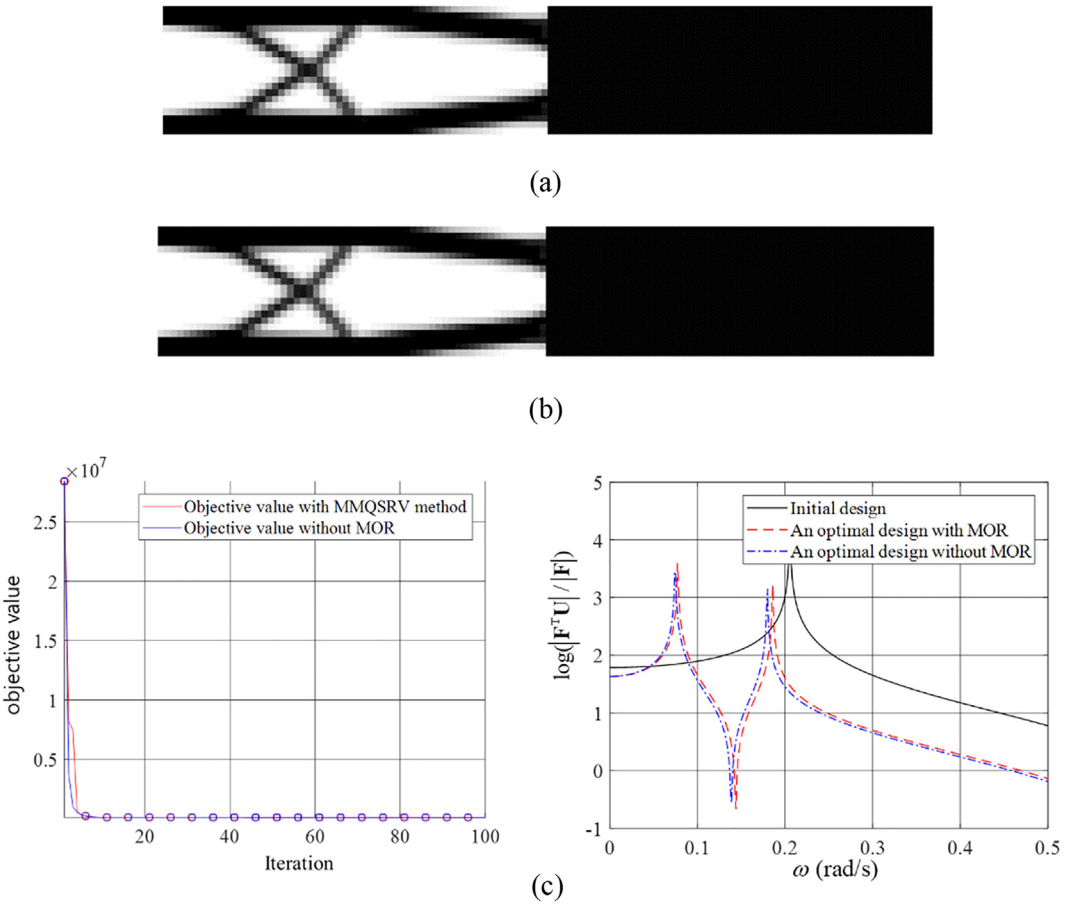

Fig. 9. Dynamic compliance minimization for the low-frequency domain with same Young's moduli ($E_1 = 10$ Pa, $E_2 = 10$ Pa, $\omega_s = 0$ rad/s, $\omega_e = 0.01$ rad/s, $\Delta\omega = 10^{-5}$ rad/s), (a) the optimal layout with the MOR scheme, $\Phi = 1.0015 \times 10^5$ (m · rad/s), computing time = 2.6634×10^3 s (100 iterations), (b) the optimal layout without the MOR, $\Phi = 1.0000 \times 10^5$ (m · rad/s), computing time = 1.1231×10^4 s (100 iterations), and (c) the objective history and the frequency response analysis.

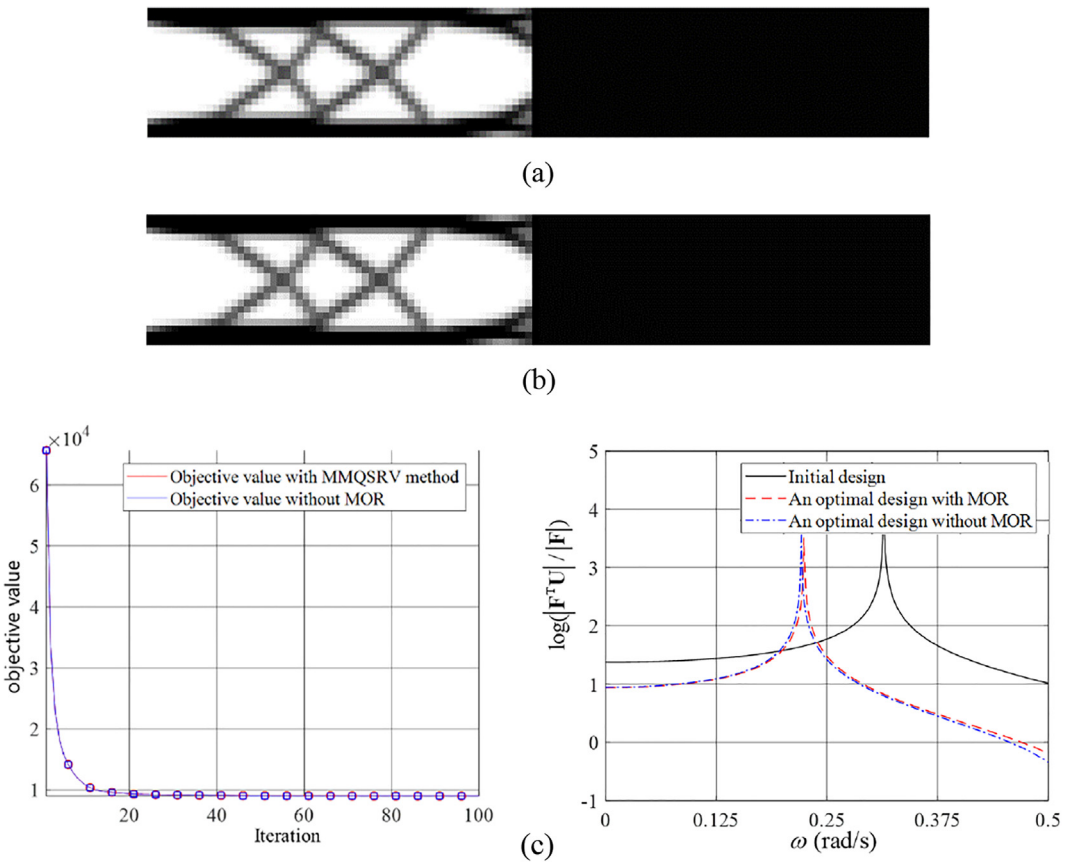

Fig. 10. Dynamic compliance minimization for the low-frequency domain with different Young's moduli ($E_1 = 1000$ Pa, $E_2 = 10$ Pa, $\omega_s = 0$ rad/s, $\omega_e = 0.01$ rad/s, $\Delta\omega = 10^{-5}$ rad/s), (a) the optimal layout with the MOR scheme, $\Phi = 8.8973 \times 10^3$(m · rad/s), computing time = 2.6417×10^3 s (100 iterations), (b) the optimal layout without the MOR scheme, $\Phi = 8.9890 \times 10^3$(m · rad/s), computing time = 1.1330×10^4 s (100 iterations), and (c) the objective history and frequency response analysis.

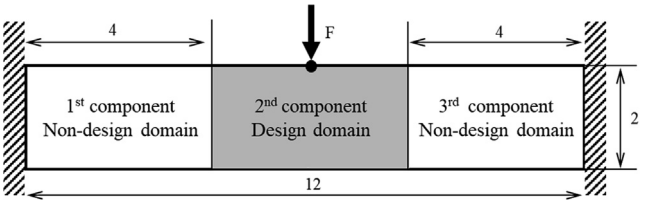

Fig. 11. Two-dimensional cantilever beam (120×20 Q4 elements, $E_1 = E_2 = E_3 10$ Pa, $v = 0.3$, $\rho = 1$ kg/m^3, basic thickness = 1, reinforcement thickness = 1) with three subcomponents.

$$\max(|\Phi_{\text{iter}} - \Phi_{\text{iter - 1}}|) < 10^{-4}, \text{ Maximum iteration } = 100, \quad (63)$$

where the iteration number is denoted by iter. In order to compare the computation time, the total optimization time with the finite element procedure is measure for 100 optimization iterations.

4.1. Example 1: cantilever beam with two domains

For the first example, the topology optimization of minimizing the dynamic compliance of a simple cantilever beam with 1 thickness is considered in Fig. 8(a). The design domain is discretized into 120×20 Q4 elements. The left side is clamped and a point load (F = 1 N) is applied to the bottom-right corner. Note that the conventional topology optimization designs the total domain whereas this study topologically designs only the left side of the analysis domain. This example considers two kinds of cases. For the first case, the Young's moduli of the domains are set to c while the first component has a 100 times higher Young's modulus than that of the second component ($E_1 = 10$ Pa, $E_2 = 10$ Pa) for the second case. The Poisson's ratio and density of the solid are set to 0.3 and 1 Kg/m^3, respectively. To save on computation time, the MOR approach for multiple components with the quasi-static Ritz vector approach at multiple frequencies (MMQSRV method) is applied. The topology optimization process using the MOR method is shown in Fig. 7 [29]. The 2562 degrees of freedom of the left side is reduced to 126 and the 42 degrees of freedom of the interface line is preserved. The optimization formula is then defined as follows.

$$\begin{aligned} &\min_{\gamma} \quad \Phi = \int_{\omega_s}^{\omega_e} \left|\mathbf{F}^T\mathbf{X}\right| d\omega, \\ &\text{S.t.} \quad \sum_{i=1}^{NE} \gamma_i v_i \leqslant V^* = 0.3V_0 \end{aligned}, \quad (64)$$

where the design variable and volume of the i-th element are γ_i and v_i, respectively. The total number of elements is $NE = 2400$ (120×20). The volume limit V^* is constrained to be less than 30% of the initial design domain volume. The dynamic compliance for the low frequency range [0, 0.01] (rad/s) (located at the left side of the first resonance frequency of the initial design with $\gamma_i = 1$) is minimized with and without the MMQSRV method for case 1 ($E_1 = 10$ Pa, $E_2 = 10$ Pa) and case 2 ($E_1 = 1000$ Pa, $E_2 = 10$ Pa) in Fig. 9 and Fig. 10, respectively. Because the frequency domain is set to [0, 0.01] (rad/s), the center frequencies are equally set to [0 0.005 0.01] (rad/s) for the MMQSRV method.

Fig. 9(a) and Fig. 10(a) show the layout of the topology optimization and the value of objective function at each iteration. Comparing the results, it is verified that the topology optimization

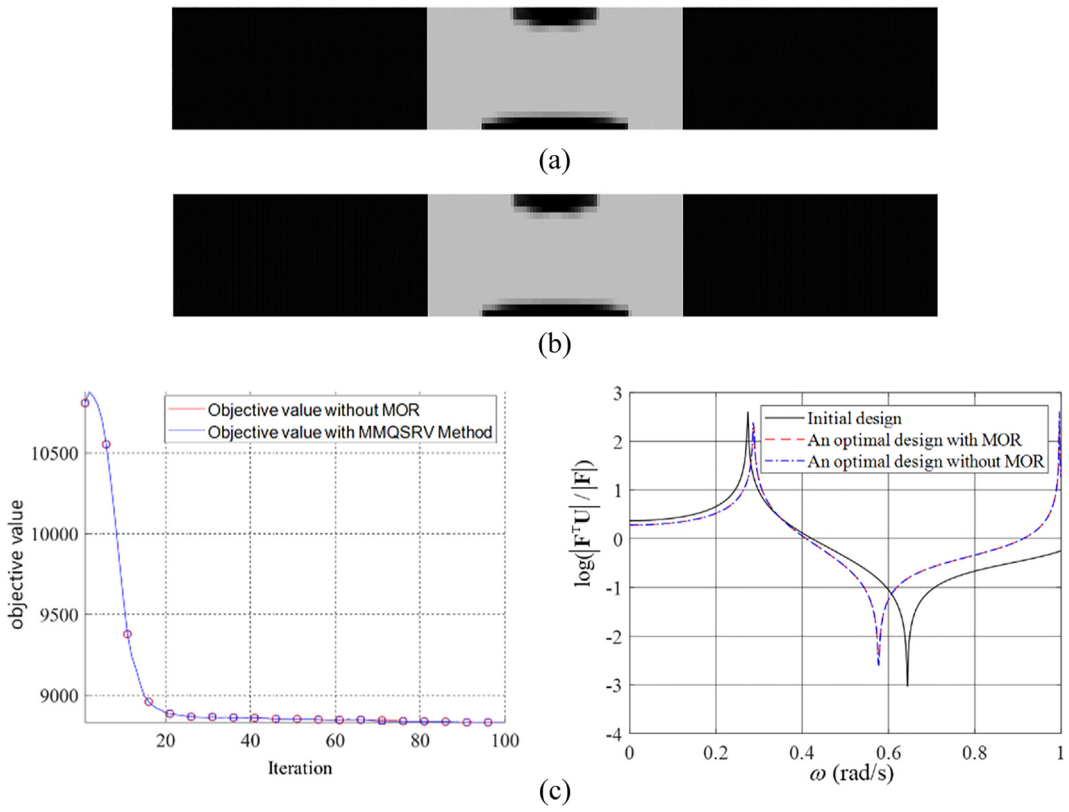

Fig. 12. Dynamic compliance minimization for the first frequency domain, ($\omega_s = 0$ rad/s, $\omega_e = 0.2$ rad/s, $\Delta\omega = 10^{-5}$ rad/s), (a) the optimal layout with the MOR approach, $\Phi = 9.0142 \times 10^3$ (m · rad/s), computing time = 1.1318×10^4 s (100 iterations), (b) the optimal layout without the MOR approach, $\Phi = 9.0070 \times 10^3$ (m · rad/s), computing time =4.4543×10^4 s (100 iterations), and (c) the objective history and frequency response analysis.

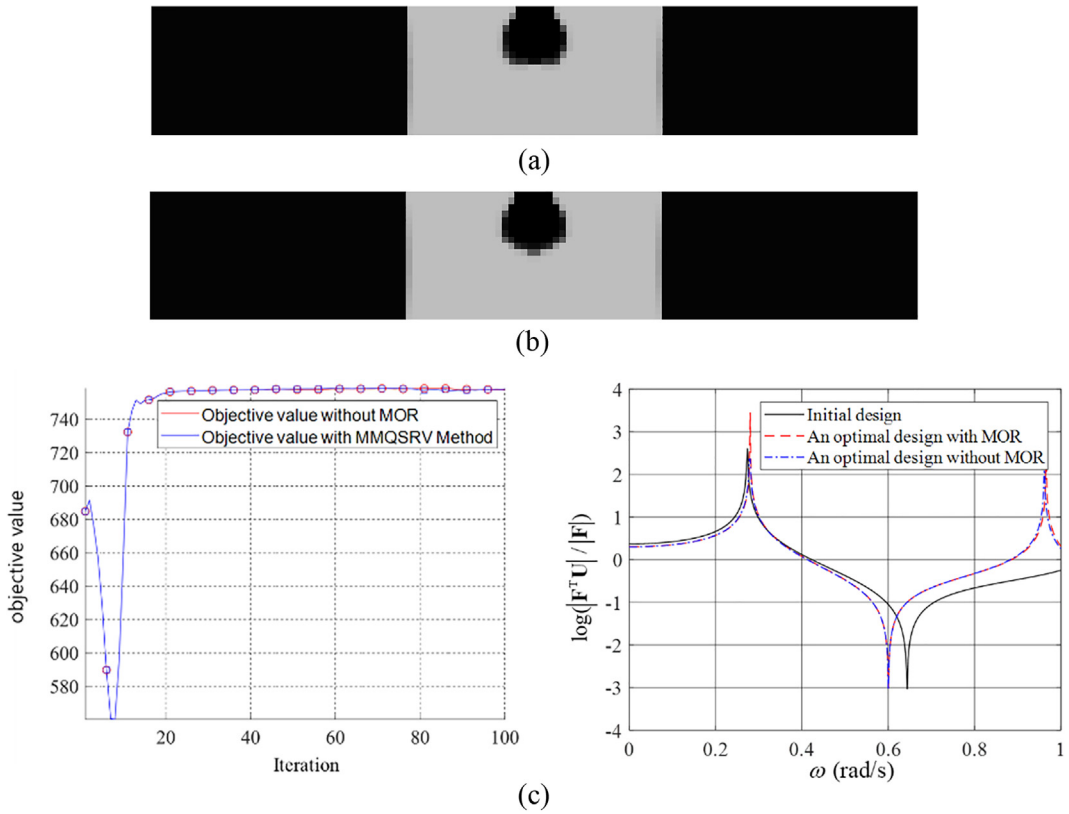

Fig. 13. Dynamic compliance minimization for the second frequency domain, ($\omega_s = 0.4$ rad/s, $\omega_e = 0.6$ rad/s, $\Delta\omega = 10^{-5}$ rad/s) (a) the optimal layout with the MOR approach, $\Phi = 1.6346 \times 10^3$ (m · rad/s), computing time = 1.1080×10^4 s (100 iterations), (b) the optimal layout without the MOR approach, $\Phi = 1.5592 \times 10^3$ (m · rad/s), computing time =4.5756×10^4 s (100 iterations), and (c) the objective history and frequency response analysis.

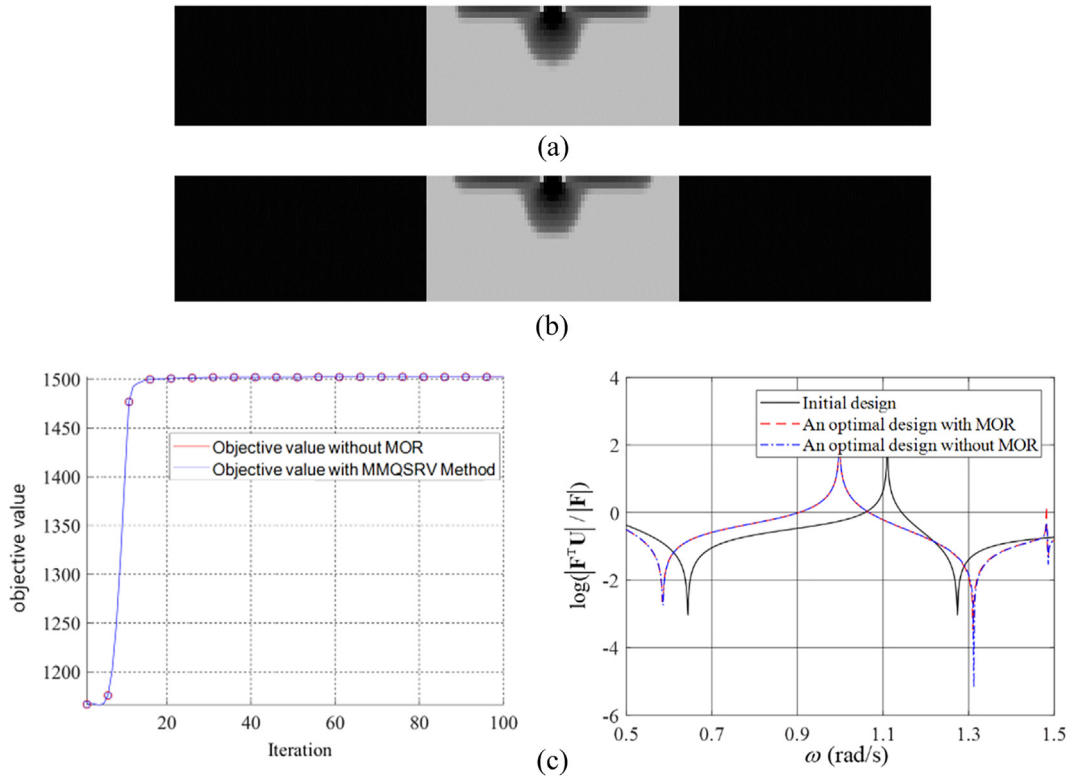

Fig. 14. Dynamic compliance minimization for the higher frequency domain, ($\omega_s = 1.1$ rad/s, $\omega_e = 1.3$ rad/s, $\Delta\omega = 10^{-5}$ rad/s) (a) the optimal layout with the MOR approach, $\Phi = 1.0402 \times 10^3$(m rad/s), computing time = 1.1083×10^4 s, (b) the optimal layout without the MOR approach, $\Phi = 1.0972 \times 10^3$(m rad/s), computing time = 4.5889×10^4 s (100 iterations), and (c) the objective history and frequency response analysis.

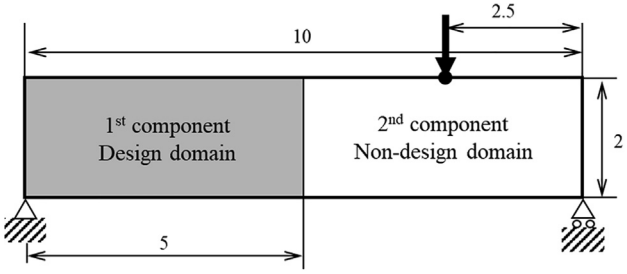

Fig. 15. Two-dimensional MBB beam (120×20 Q4 elements, $v = 0.3$, $\rho = 1$ kg/m^3) with two subcomponents.

layout and the objective value using the MMQSRV method are almost similar to those of the TO without the MOR approach. The error indicator in equation (62) of the first optimization example are 5.2427×10^{-2} in Fig. 9 and 5.9938×10^{-4} in Fig. 10, respectively. Within these errors, the similar designs with and without the present MOR approach can be obtained. The optimal structures are similar to the designs minimizing the static compliance because minimizing the dynamic response of the considered quite low-frequency domain stiffens structure. To minimize the objective function value, the curve of the FRF shifts to the left side in Fig. 9(b). Because the stiffness of the structure is increased, the material part of the optimization layout becomes thinner which reduces material amount and reveals a new reinforcement structure in Fig. 10(a).

The total computation time for the optimization procedure with the MMQSRV method is reduced to just over one-fourth that of the computation time without the MOR for both case 1 and case 2 in Fig. 9(c) and Fig. 10(c). Examining the computation time in detail, it is found that the calculation time for FE analysis, e.g., obtaining mass, stiffness, displacement matrix, and so on, is reduced almost ten times. However, the calculation time for optimization, e.g., the objective value, the sensitivity, the optimization process, and so on, is not reduced. Therefore, the effect of model reduction scheme for time reduction in the total optimization process is weaker compared to that in the FE analysis.

4.2. Example 2: reinforcement problem

For the second optimization example, a reinforcement problem with 3 sub-structures in Fig. 11 is considered. In this example, we consider the dynamic compliance not only in the low-frequency domain but also in the high-frequency domain. To maintain the geometrical similarity with the previous examples, the design domain is discretized into 120×20 Q4 elements. However, the design variables are set to the reinforcement to minimize the dynamic compliance of the design. In other words, the basic structure with 1 thickness is reinforced by an additional layer, which has 30% of the initial design volume and a thickness of 0.5. The optimization formulation is set up as (64) with 0.3 V_0 for the volume constraint.

The first frequency domain is set to [0, 0.2] (rad/s) located at the left side of the first resonance frequency of the initial design and the second frequency domain is set to [0.4, 0.6] (rad/s) located between the first and second resonance frequencies. The third frequency domain is set to [1.1, 1.3] (rad/s) located at the right side of the second resonance frequency. The optimization problems for each frequency domain are solved with and without using the MMQSRV method in Fig. 12, Fig. 13, and Fig. 14. The error indicator in equation (62) of the second optimization examples are 2.2442×10^{-4} for Fig. 12, $1.5034 \times 10^{-2}$for Fig. 13, and

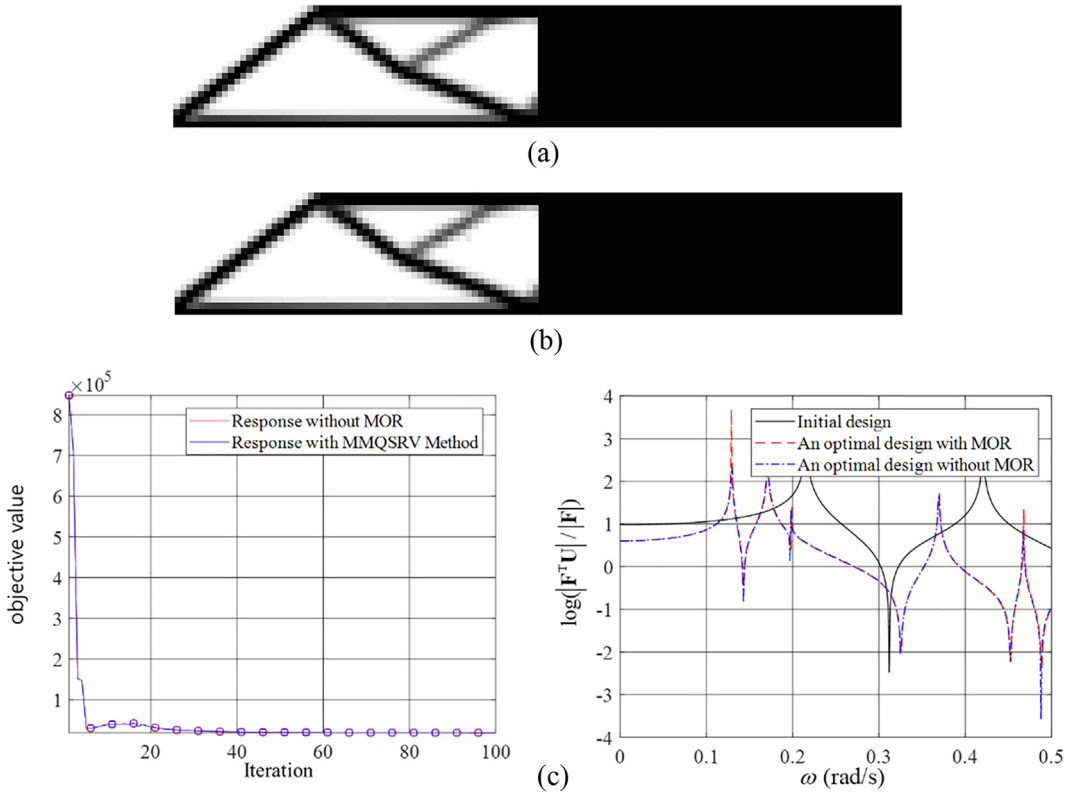

Fig. 16. Dynamic compliance minimization for the low-frequency domain, ($\omega_s = 0$ rad/s, $\omega_e = 0.1$ rad/s, $\Delta\omega = 10^{-5}$ rad/s) (a) the optimal layout with the MOR approach, $\Phi = 1.8771 \times 10^4$ (m rad/s), computing time = 4.8491×10^3 s (100 iterations), (b) the optimal layout without the MOR approach, $\Phi = 1.8822 \times 10^4$(m rad/s), computing time = 2.2159×10^4 s (100 iterations), and (c) the objective history and frequency response analysis.

3.9537×10^{-2} for Fig. 14, respectively. Owing to the accurate solutions, the designs with the MOR approach are almost identical to the designs without the MOR approach.

The FRFs of each frequency domain is optimized in order to minimize the objective value of the target frequency. Stable convergences could be obtained with the MMQSRV method in these examples. The optimal layouts are almost similar to those without the MOR approach but almost 4 times faster in Fig. 12(c), Fig. 13(c), and Fig. 14(c).

4.3. Example 3: MBB beam with two domains

To verify versatility and robustness of MMQSRV method, the 10×2 box beam problem with the loading condition in Fig. 15 is considered for the last example. The design domain is discretized into 120×20 Q4 elements. A point load (F = 1 N) is applied to the center of the 2nd component which means the external load is outside of the design domain. The two kinds of loading conditions are considered. For the first loading case, the low-frequency domain (cc) for dynamic compliance is considered and for the second case, the higher frequency domain ($\omega_s = 0.3$ rad/s, $\omega_e = 0.4$ rad/s) is considered. The objective function and the constraint are formulated in (64). The results with and without the MMQSRV method are shown in Fig. 16 and Fig. 17, respectively. In Fig. 16(a), it can be verified that the optimized layout and the objective value at each iteration are similar to each other. However, for the second frequency domain, i.e., [0.3 0.4] (rad/s), some differences are observed due to the insufficient accuracy. During an optimization process, these discrepancies in responses affect the optimization processes and the different local optimal layouts are obtained. It also shows that the numerical error of the MOR method causes grey elements [32,33]. The objective values and the computation times can be found in Fig. 16 and Fig. 17. The error indicator in (62) of the third optimization example are 2.3397×10^{-2} in Fig. 16, 2.2614×10^{-1} in Fig. 17(a), and 1.4623×10^{-1} in Fig. 17 (b), respectively. In this example, for the higher frequency response, the higher error in the finite element response causes some discrepancies in optimum designs. To reduce the errors, it is possible to increase the number of bases and it is possible to obtain the similar responses and the associated similar designs.

5. Conclusion

This paper presents a new model order reduction method and develops the density-based topology optimization using this MOR approach. In of the dynamic response of a complex manifold composed of multi-substructures, the efficient calculation of dynamic responses is very important. Therefore the model order reduction scheme has been introduced. This study investigated in detail the applications of MOR schemes for topology optimization of multi-component dynamic system and a new MOR approach. The new MOR method named as the Multi-substructure Multi-frequency Quasi-Static Ritz Vector (MMQSRV) method scheme has a distinct and unique way of constructing reduction bases for approximating the structural response. It calculates its basis functions by considering not only external force, mass, and stiffness matrices but also pseudo-loads along interface line or surface. We also validate the accuracy and efficiency of the MMQSRV method by comparing it with earlier methods such as RV, QSRV, and MQSRV. Then it is possible to use the MMQSRV method for the dynamic structural topology optimization problem wherein the optimization design domain is a subpart of the whole structure. With several topology optimization examples, it is illustrated that the computational efficiency can be improved compared to the full

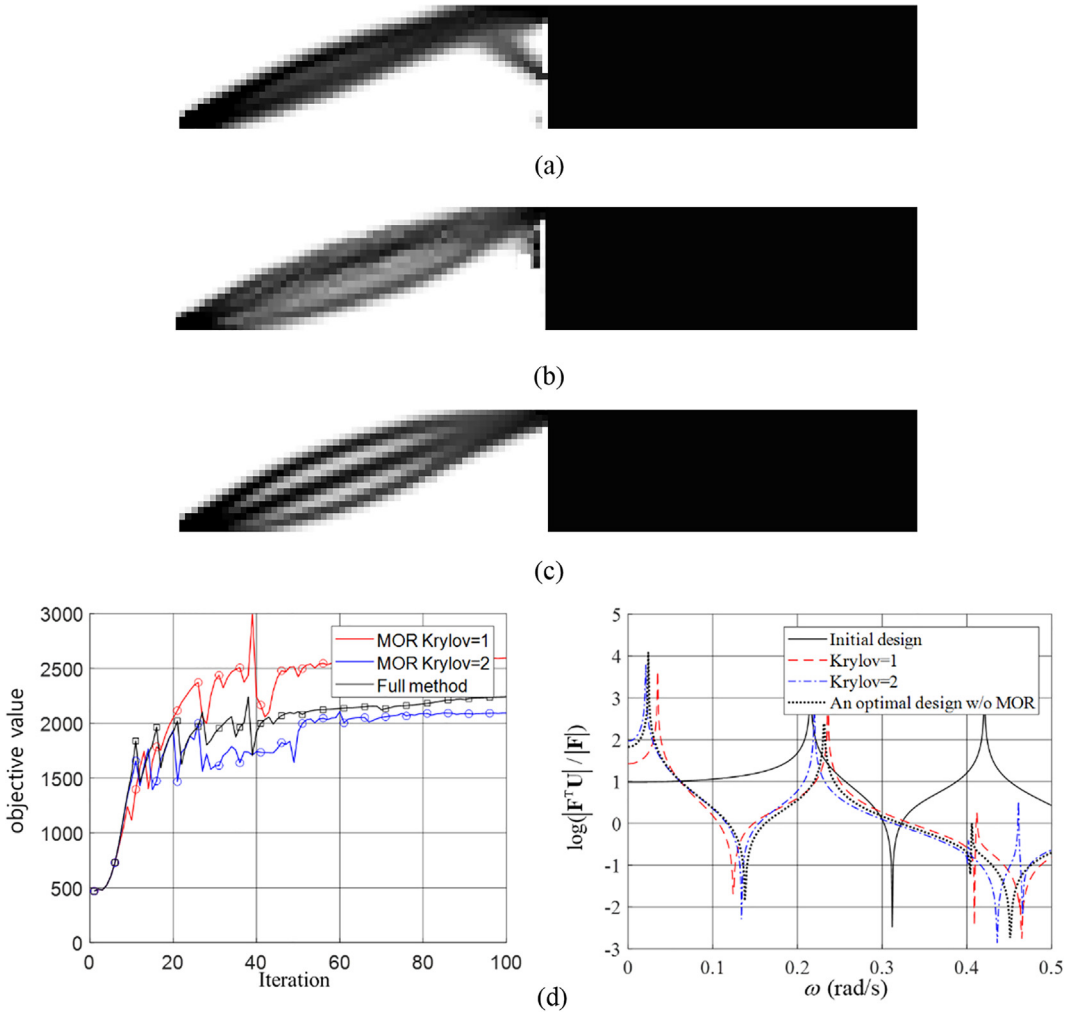

Fig. 17. Dynamic compliance minimization for the higher frequency domain, ($\omega_s = 0.3$ rad/s, $\omega_e = 0.4$ rad/s, $\Delta\omega = 10^{-5}$ rad/s) (a) the optimal layout with the MOR approach (1 Krylov subspace), $\Phi = 2.5926 \times 10^3$(m rad/s), iteration = 100, computing time = 4.8380×10^3 s (100 iterations), (b) the optimal layout with the MOR approach (2 Krylov subspace), $\Phi = 2.6225 \times 10^3$(m rad/s), computing time = 7.1858×10^3 s (100 iterations), (c) the optimal layout without the MOR approach, $\Phi = 2.2416 \times 10^3$(m rad/s), computing time = 2.1671×10^4 s (100 iterations), and (d) the objective history and frequency response analysis.

optimization results. The advantage of the MMQSRV method is increased with more complex geometry and more degrees of freedom. In conclusion, this research presents a new MOR method and finds that this new MOR method can efficiently achieve topology optimization for dynamic systems.

Declaration of Competing Interest

There is no conflict of interest of this research

Acknowledgement

This work was supported by the National Research Foundation of Korea (NRF) grant funded by the Korea government (MSIT) (NRF-2019R1A2C2084974).

Appendix A. Supplementary material

Supplementary data to this article can be found online at https://doi.org/10.1016/j.compstruc.2019.106146.[1]

[1] This work was supported by the National Research Foundation of Korea (NRF) grant funded by the Korea government (MSIT) (NRF-2019R1A2C2084974).

References

[1] Bathe KJ. Finite element procedures. Prentice Hall; 1996. p. 1037.
[2] Bendsøe MP, Sigmund O. Topology optimization: theory, methods and applications. 2003. Springer; 2013.
[3] Cornwell RE, Craig Jr RR, Johnson CP. On the application of the mode-acceleration method to structural engineering problems. Earthquake Eng Struct Dyn 1983;11:679–88.
[4] Craig RR, Bampton MCC. Coupling of substructures for dynamic analyses 1968;6:1313–9.
[5] Ghasemi H, Park HS, Rabczuk T. A level-set based IGA formulation for topology optimization of flexoelectric materials. Comput Methods Appl Mech Eng 2017;313:239–58.
[6] Ghasemi H, Park HS, Rabczuk T. A multi-material level set-based topology optimization of flexoelectric composites. Comput Methods Appl Mech Eng 2018;332:47–62.
[7] Gogu C. Improving the efficiency of large scale topology optimization through on-the-fly reduced order model construction. Int J Numer Methods Eng 2015;101:281–304.
[8] Gu J, Ma ZD, Hulbert GM. A new load-dependent Ritz vector method for structural dynamics analyses: quasi-static Ritz vectors. Finite Elem Anal Des 2000;36:261–78.
[9] Guyan RJ. Reduction of stiffness and mass matrices. AIAA J 1965;3:380.
[10] Jang HH, Lee HA, Lee JY, Park GJ. Dynamic response topology optimization in the time domain using equivalent static loads. AIAA J 2012;50:226–34.
[11] Jensen JS. Topology optimization of dynamics problems with Padé approximants. Int J Numer Methods Eng 2007;72:1605–30.
[12] Kim J-G, Lee P-S. An enhanced Craig-Bampton method. Int J Numer Methods Eng 2015;103:79–93.

[13] Kim JG, Boo SH, Lee CO, Lee PS. On the computational efficiency of the error estimator for Guyan reduction. Comput Methods Appl Mech Eng 2016;305:759–76.
[14] Lee KS, Geem ZW. A new structural optimization method based on the harmony search algorithm. Comput Struct 2004;82:781–98.
[15] Léger P, Wilson EL. Generation of load dependent Ritz transformation vectors in structural dynamics. Eng Comput 1987;4:309–18.
[16] Liang YC, Lee HP, Lim SP, Lin WZ, Lee KH, Wu CG. Proper orthogonal decomposition and its applicationspart i: theory. J Sound Vib 2002;252:527–44.
[17] Liu H, Zhang W, Gao T. A comparative study of dynamic analysis methods for structural topology optimization under harmonic force excitations. Struct Multidiscipl Optimiz 2015;51:1321–33.
[18] Liu T, Zhu JH, Zhang WH, Zhao H, Kong J, Gao T. Integrated layout and topology optimization design of multi-component systems under harmonic base acceleration excitations. Struct Multidiscipl Optimiz 2019;59:1053–73.
[19] Ma ZD, Kikuchi N, Hagiwara I. Structural topology and shape optimization for a frequency response problem. Comput Mech 1993;13:157–74.
[20] Ma ZD, Kikuchi N, Pierre C, Raju B. Multi-domain topology optimization for vehicle substructure design. In: ASME 2002 International Mechanical Engineering Congress and Exposition American Society of Mechanical Engineers. p. 12–20.
[21] Mediante EC, Jensen JS, Brunskog J, Larsen M. Reduced order modeling in topology optimization of vibroacoustic problems. The Journal of the Acoustical Society of America 2017;141:4035.
[22] Ricles JM, Léger P. Use of load-dependent vectors for dynamic analysis of large space structures. Commun Numer Methods Eng 1993;9:897–908.
[23] Rong JH, Xie YM, Yang XY, Liang QQ. Topology optimization of structures under dynamic response constraints. J Sound Vib 2000;234:177–89.
[24] Shu L, Wang MY, Fang Z, Ma Z, Wei P. Level set based structural topology optimization for minimizing frequency response. J Sound Vib 2011;330:5820–34.
[25] Wang MY, Wang X, Guo D. A level set method for structural topology optimization. Comput Methods Appl Mech Eng 2003;192:227–46.
[26] Wilson EL, Yuan MW, Dickens JM. Dynamic analysis by direct superposition of Ritz vectors. Earthquake Eng Struct Dyn 1982;10:813–21.
[27] Xia L, Breitkopf P. A reduced multiscale model for nonlinear structural topology optimization. Comput Methods Appl Mech Eng 2014;280:117–34.
[28] Yao MS. Nonlinear structural dynamic finite element analysis using Ritz vector reduced basis method. Shock Vib 1996;3.
[29] Yoon GH. Structural topology optimization for frequency response problem using model reduction schemes. Comput Methods Appl Mech Eng 2010;199:1744–63.
[30] Yoon GH. Toward a multifrequency quasi-static Ritz vector method for frequency-dependent acoustic system application. Int J Numer Methods Eng 2012;89:1451–70.
[31] Yoon GH, Kim JH, Jung KO, Jung JW. Transient quasi-static Ritz vector (TQSRV) method by Krylov subspaces and eigenvectors for efficient contact dynamic finite element simulation. Appl Math Model 2015;39:2740–62.
[32] Zhao J, Wang C. Dynamic response topology optimization in the time domain using model reduction method. Struct Multidiscipl Optimiz 2016;53:101–14.
[33] Zhao J, Wang C. Topology optimization for minimizing the maximum dynamic response in the time domain using aggregation functional method. Comput Struct 2017;190:41–60.